

**CONFORMATION STUDY AND CRYSTAL STRUCTURE
OF $C_{29}H_{25}N_3O_3$**

136811

**A Thesis Submitted to the
Graduate School of Natural and Applied Sciences of
Dokuz Eylül University
In Partial Fulfillment of the Requirements for
The Degree of Master of Science in Physics**

**by
Hasan KARABIYIK**

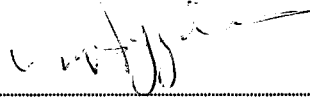
**July, 2003
İZMİR**

**İZ. YÜKSEKÖĞRETİM KURULU
DOKÜMANLARA BAKIM**

136811

Ms.Sc. THESIS EXAMINATION RESULT FORM

We certify that we have read the thesis, entitled “**CONFORMATION STUDY AND CRYSTAL STRUCTURE OF C₂₉H₂₅N₃O₃**” completed by **HASAN KARABIYIK** under supervision of **ASSIST. PROF. DR. MUHİTTİN AYGÜN** and that in our opinion it is fully adequate, in scope and in quality, as a thesis for the degree of Master of Science.



Assist. Prof. Dr. Muhittin Aygün

Supervisor



Prof. Dr. Kemal Kocabaş

Committee Member



Assoc. Prof. Dr. Serap Alp

Committee Member

Approved by the
Graduate School of Natural and Applied Sciences



Prof. Dr. Cahit Helvacı

Director

**T.C. YÜSEKÖĞRETİM KURULU
DOKÜMANTASYON MERKEZİ**

ACKNOWLEDGEMENTS

I would like to express my deepest gratitude to my supervisor Assistant Prof. Muhittin AYGÜN for his continual presence, invaluable guidance and endless patience throughout the course of this work and especially to accept me as his pupil.

I am greatly indebted to Necdet COŞKUN for his invaluable helping in chemical supports.

I also would like to thank to Aytaç Gürhan GÖKÇE for his technical supports and my other roommates Ümit AKINCI, Cenk AKYÜZ and Gül GÜLPINAR for close friendships.

Finally, my deepest gratitude goes to my family whose constant support, patience made me keep going.

Hasan KARABIYIK

ABSTRACT

The *cis* stereochemistry of 6-(4-methoxy-phenyl)-1,5,7a-triphenyl-tetrahydroimidazo [1,5-b][1,2,4] oxadiazol-2-one was studied by AM1 and PM3 semi-empirical quantum mechanical models at restricted Hartree-Fock level and X-ray crystallographic analysis. It crystallizes in the monoclinic space group $P2_1/n$ with $a = 10.812(1) \text{ \AA}$, $b = 16.464(2) \text{ \AA}$, $c = 13.379(1) \text{ \AA}$, $\alpha = 90.00^\circ$, $\beta = 98.39(1)^\circ$, $\gamma = 90.00^\circ$, $V = 2356.07(4) \text{ \AA}^3$, $Z = 4$, $D_{\text{calc}} = 1.3067 \text{ g/cm}^3$, $F(000) = 976.41$, $\mu = 0.086 \text{ mm}^{-1}$. The structure was solved by direct methods and refined to $R(\text{obs}) = 0.066$ for 1257 independent reflections [$I > 4\sigma(I)$]. The results from X-ray diffraction were seen to be in generally consistence with theoretical calculations except for conformation of the five membered heterocyclic rings. One of the five membered rings through O2, N2, C3, N3, and C4 atoms is in twisted conformation and the other through N1, C1, N2, C3, and C2 atoms are in envelope conformation. C1 atom has maximum deviation [$-0.291(5) \text{ \AA}$] from average ring plane of enveloped five membered ring. C18...C23 and C12...C17 phenyl rings are attached to the five membered ring under discussion as bisectonal (neither equatorial nor axial) and equatorial respectively. 4-methoxyphenyl ring is equatorially linked to this ring, and finally, phenyl ring C24...C29 is also equatorially attached to the twisted five membered ring. Two inter- and intramolecular weak interactions in addition to two asymmetric carbon atoms were found in the structure. To investigate conformational flexibility of the title molecule, heat of formation values belonged to each conformer corresponding to certain values of selected four torsion angles were computed by varying in every 10° , after the isolated (or free) molecular structure was optimized.

ÖZET

6-(4-metoksi-fenil)-1,5,7a-trifenil-tetrahidro-imidazo [1,5-b][1,2,4] oksa diazolu-2-on bileşiğinin cis stereokimyası ve biçimlenimsel analizi sırasıyla tek kristal X-ışını yöntemi ve sınırlandırılmış Hartree-Fock düzeyindeki AM1 ve PM3 yarı deneysel kuantum mekaniksel modeller kullanılarak gerçekleştirildi. Yukarıda adı geçen molekül $P2_1/n$ uzay grubunda monoklinik paketleme sisteminde $a = 10.812(1)$ Å, $b = 16.464(2)$ Å, $c = 13.379(1)$ Å, $\alpha = 90.00^\circ$, $\beta = 98.39(1)^\circ$, $\gamma = 90.00^\circ$, $V = 2356.07(4)$ Å³, $Z = 4$, $D_{\text{calc}} = 1.3067$ g/cm³, $F(000) = 976.41$, $\mu = 0.086$ mm⁻¹ şeklinde sıralanabilecek kristalografik parametrelere sahip olarak kristalleşmiştir. Moleküler ve kristalografik yapı doğrudan yöntemlerle çözüldü ve $I > 4\sigma(I)$ koşulunu sağlayan 1257 bağımsız yansıma için $R(\text{göz.})=0.066$ değerine arıtıldı. X-ışını kırınımından elde edilen sonuçların beş üyeli heterosiklik halkaların konformasyonları dışında teorik hesaplamalarla genel bir uyum içinde olduğu görüldü. O2, N2, C3, N3 ve C4 atomlarının tanımladığı beş üyeli halka bükülmüş konformasyonda yer alırken N1, C1, N2, C3 ve C2 atomlarının tanımladığı diğer beş üyeli halka ise zarf konformasyonundadır. C1 atomu zarf konformasyonundaki halkadan konumsal olarak en büyük sapmaya [0.291(5) Å] sahiptir. C18...C23 ve C12...C17 fenil halkaları sözkonusu bu beş üyeli halkaya sırasıyla eştarafli (aksiyal ya da ekvatoryal olmayan) ve ekvatoryal olarak bağlanmıştır. 4-metoksi fenil halkası da zarf konformasyonundaki halkaya ve son olarak C24...C29 fenil halkası da bükülmüş beş üyeli halkaya ekvatoryal olarak bağlanmıştır. Molekül iki tane asimetric karbon atomu barındırmakla beraber iki tane molekül içi ve iki tane de moleküller arası zayıf etkileşime sahiptir. Molekülün biçimlenimsel esnekliğini incelemek için, serbest molekül optimize edildikten sonra, seçilen dört burulum açısının değeri her 10⁰ de bir değiştirilerek elde edilen konformerlerinin oluşum enerjileri hesaplandı.

CONTENTS

	Page
Contents.....	vii
List of Figures.....	xi
List of Tables.....	xiii

Chapter One

INTRODUCTION

1.1	
Introduction.....	1

Chapter Two

X-RAY DIFFRACTION DATA

2.1 Measurement Methods of Diffraction Intensities.....	5
2.2 Scattering of X-rays by a Crystal.....	6
2.3 Crystal Structure Factor.....	8
2.4 Fourier Synthesis and Electron Density.....	9
2.5 Data Reduction.....	10
2.5.1 Lorentz Correction.....	11
2.5.2 Polarisation Correction.....	11
2.5.3 Absorption Correction.....	12
2.5.4 Debye-Waller Temperature Factor Correction.....	13
2.5.5 Extinction Correction.....	15
2.5.6 Anomalous Scattering Factor.....	15

Chapter Three

SOLUTION OF CRYSTAL STRUCTURE

3.1 Introduction.....	17
3.2 The Phase Problem.....	17
3.3 The trial-and-error method.....	19
3.4 The Patterson Technique.....	19
3.5 Direct Methods.....	19
3.5.1 Normalized Structure Factors and Intensity Statistics.....	20
3.5.2 Fundamental Formulae.....	21
3.6 Criteria of Correctness Set of Phases.....	27
3.6.1 MABS.....	27
3.6.2 NQUAL.....	28
3.6.3 R_{α} FOM.....	28

Chapter Four

CRYSTAL STRUCTURE REFINEMENT

4.1 Refinement Methods.....	29
4.1.1 Difference Fourier Method.....	29
4.1.2 Least-Squares Method.....	30
4.1.2.1 Overall Strategy.....	31
4.2 Error Analysis.....	32
4.2.1 R Factors.....	32
4.2.2 Goodness of Fit.....	32
4.2.3 Final Difference Map.....	32
4.2.4 Estimated Standard Deviations.....	33

Chapter Five

COMPUTATIONAL METHODS

5.1 What is the Computational Chemistry?.....	34
---	----

5.2 Molecular Mechanics.....	35
5.3 Energy Calculation.....	36
5.3.1 Bond Stretch.....	37
5.3.2 Bond Angles.....	38
5.3.3 Dihedral Angles.....	39
5.3.4 Non-bonded Interactions.....	39
5.3.5 Other terms.....	41
5.4 Quantum Mechanical Calculations.....	41
5.4.1 SCF Theory.....	42
5.4.2 Configuration Interaction.....	43
5.4.3 <i>Ab Initio</i> Method.....	44
5.4.4 Neglecting Differential Overlap (NDO).....	46
5.4.5 Semi-empirical Methods.....	47
5.4.5.1 AM1 Method.....	48
5.4.5.2 PM3 Method.....	50

Chapter Six

COMPUTATION TYPES

6.1 Introduction.....	52
6.2 Single Point Calculation.....	52
6.3 Geometry Optimization.....	53
6.3.1 Steepest Descent.....	54
6.3.2 Conjugate Gradient.....	54
6.3.3 Block Diagonal.....	55
6.3.4 Eigenvector Following.....	55

Chapter Seven

EXPERIMENTAL DETAILS

7.1 The Crystal of $C_{29}H_{25}N_3O_3$	56
7.1.1 Data Collection of $C_{29}H_{25}N_3O_3$ Crystal.....	56

7.1.2 Structure Solution & Refinement of $C_{29}H_{25}N_3O_3$ Crystal.....	57
7.1.3 Experimental Results for $C_{29}H_{25}N_3O_3$ Crystal.....	57
7.1.4 Molecular Graphics of $C_{29}H_{25}N_3O_3$ Crystal.....	67
7.2 Computational Details for the Molecule.....	71

Chapter Eight

CONCLUSIONS

8.1 Conclusions Related to X-Ray Crystallographic Studies.....	77
8.2. Conclusions Related to Computational Aspects.....	78
References.....	83



LIST OF FIGURES

		Page
Figure 1.1	The chemical diagram of 6-(4-methoxy-phenyl)-1,5,7a-triphenyl-tetrahydro-imidazo[1,5- <i>b</i>][1,2,4] oxadiazol-2-one.....	1
Figure 1.2	The chemical diagram of compound A with groups that can be substituted various functional structures.....	2
Figure 1.3	Chemical Diagram of Compounds 1 with groups that can be substituted various functional structures.....	3
Figure 2.1	Diffraction scan types. (a) w -scan (b) $w/2\theta$ -scan.....	6
Figure 2.2	Combination of N waves on an Argand diagram.....	7
Figure 2.3	Atomic scattering factors: (a) stationary atom, (b) atom corrected for thermal vibration.....	9
Figure 2.4	Wilson plot.....	15
Figure 2.5	Anomalous scattering of atom A with respect to the rest of the structure R: (a) normal case- $ F(h) = F(\bar{h}) $; (b) anomalous case $ F(h) \neq F(\bar{h}) $	16
Figure 5.1	Morse Potential and Harmonic Potential.....	37
Figure 5.2	Variation of energy with dihedral angle for one (--), two (··) and Threefold.....	39
Figure 5.3	Energy values versus internuclear separation.....	46
Figure 7.1	An ORTEP3 drawing of C ₂₉ H ₂₅ N ₃ O ₃ showing the intramolecular weak interactions. Displacement ellipsoids of non-H atoms are shown at the 30% probability level.....	68
Figure 7.2	Unit cell contents with the weak interactions scheme indicated by dashed lines via PLUTON program.....	69

Figure 7.3	A CPK drawing $C_{29}H_{25}N_3O_3$	70
Figure 7.4	Calculated energy profiles of the molecule by AM1 and PM3 semi-empirical method with respect to T1.....	74
Figure 7.5	Calculated energy profiles of the molecule by AM1 and PM3 semi-empirical method with respect to T2.....	75
Figure 7.6	Calculated energy profiles of the molecule by AM1 and PM3 semi-empirical method with respect to T3.....	75
Figure 7.7	Calculated energy profiles of the molecule by AM1 and PM3 semi-empirical method with respect to T4.....	76



LIST OF TABLES

	Page
Table 2.1	Atomic mass and mass absorption coefficients for $C_{29}H_{25}N_3O_3$12
Table 3.1	Some statistical properties of normalized structure factor magnitudes.....21
Table 3.2	Probabilities for the sign relationship calculated for various parameters E and N26
Table 5.1	AM1 parameters for C, H, O and N atoms.....49
Table 5.2	GCF parameters for PM3 and AM1 methods.....51
Table 7.1	FOM values for $C_{29}H_{25}N_3O_3$57
Table 7.2	Crystallographic data for $C_{29}H_{25}N_3O_3$57
Table 7.3	Atomic coordinates and equivalent isotropic thermal parameters.....59
Table 7.4	Anisotropic displacement parameters of non-hydrogen atoms.....60
Table 7.5	Bond distances in the molecule.....61
Table 7.6	Bond Angles in the molecule.....62
Table 7.7	Torsion angles in the molecule.....64
Table 7.8	Weak interactions to be regarded as weak hydrogen bonds.....66
Table 7.9	Standard deviations of atoms from the some remarkable planes.....66
Table 7.10	Dihedral angles between the planes.....67
Table 7.11	Conformational energy values versus torsion angles from -180° to $+180^\circ$ by AM1 semi-empirical method.....71
Table 7.12	Conformational energy values versus torsion angles from -180° to $+180^\circ$ by PM3 semi-empirical method.....73
Table 8.1	Selected bond distances (\AA) and bond angles ($^\circ$) with ESDs in parentheses and their values calculated by AM1 and PM3 semi-empirical method.....79

CHAPTER ONE

INTRODUCTION

1.1 Introduction

In this research, the crystal structure of 6-(4-methoxy-phenyl)-1,5,7a-triphenyl-tetrahydro-imidazo[1,5-*b*][1,2,4] oxadiazol-2-one, $C_{29}H_{25}N_3O_3$, which is incorporated one of the new compounds class, which is called as 5, 6, 7a-tetrahydroimidazo [1,5-*b*][1,2,4] oxadiazol-2 (1H)-ones by cycloadditions of Δ^3 -imidazoline 3-oxides with aryl isocyanates and thermally or photochemically induced retro cycloadditions reaction of compound A, as shown in Figure 1.2, was determined and investigated by single crystal X-ray diffraction technique and its molecular flexibility was investigated by AM1 and PM3 semi-empirical molecular orbital theories (Dewar et al., 1985; Stewart, 1989). The chemical diagram of the compound is given in Figure 1.1.

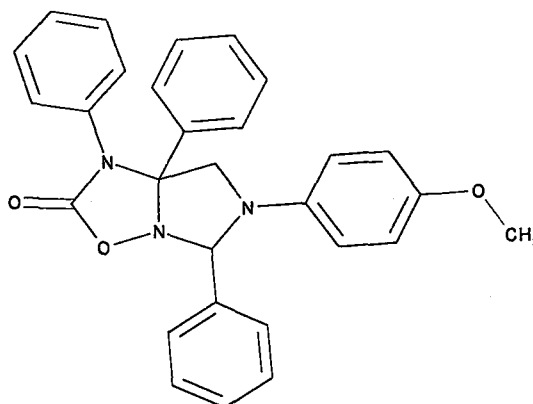


Figure 1.1 The chemical diagram of 6-(4-methoxy-phenyl)-1,5,7a-triphenyl-tetrahydro-imidazo[1,5-*b*][1,2,4] oxadiazol-2-one.

1,3-Dipolar cycloaddition reactions are excellent for the synthesis of five membered heterocyclic rings (Coşkun, 1997). The commonly used 1,3-dipoles are diazoalkanes, alkyl and allyl azides, nitrile imines, nitrile ylids and nitrones (Norman, 1978).

The 1,3-dipolar cycloadditions reaction of nitrones with olefins, acetylenes, isocyanates, isothiocyanates (Coşkun, 1997), nitrile oxides (Corsaro et al., 2002) and thiocarbonyl compounds have been reported. The 1,3-dipolar cycloaddition reaction of pyridine 1-oxide with phenyl isocyanate gave 2-anilinopyridine. The C-acylnitrone type of quinoxalin-2-one 4-oxides have also been reported to react with aryl isocyanates to give 3-arylaminquinoxalin-2-ones via an oxadiazolone intermediate.

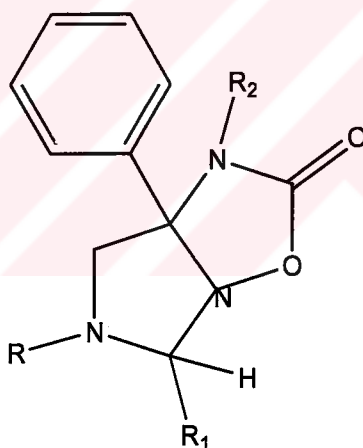


Figure 1.2 The chemical diagram of compound A with groups that can be substituted various functional structures.

Cyclic nitrones **1**, readily prepared by methods which had been already reported as professed in references (Coşkun & Sümengen, 1993), reacted with aryl isocyanates in refluxing acetonitrile or THF to give corresponding imidazooxadiazoline **A** as the sole regioisomer in excellent yields. The existence of chiral nitrones derived from D-xylose with vinyl acetate has been recently reported

in the literature (Fischer et al., 2002). The steric hindrance of the aryl group at C-2 on the nitron seems to be responsible for the approach of the 2π fragment from opposite side. The energy minimized conformations of the *cis*- and *trans*-diastereomers showed that *cis*- should be thermodynamically more stable than the *trans*. Spectral measurements about the molecule under studied had been stated in (Coşkun, 1997). ^1H NMR peaks are listed as follows: δ 3.72 (3H, s), 4.38 (2H, AB system, $J_{AB} = 11.0$), 5.88 (1H, s), 6.65 (2H, d, $J = 8.0$), 6.78 (2H, d, $J = 8.0$), 6.95 (2H, m), 7.25-7.50 (13H, m). Spin multiplicities are denoted by the symbols: s (singlet), d (doublet), m (multiplet), and J (coupling coefficient). Chemical shift values were reported in delta (δ) units, using TMS as an internal standart. The melting point of the white prisms obtained after recrystallization from acetonitrile is 143-144°C. IR (KBr) $\nu_{C=O} = 1775\text{ cm}^{-1}$.

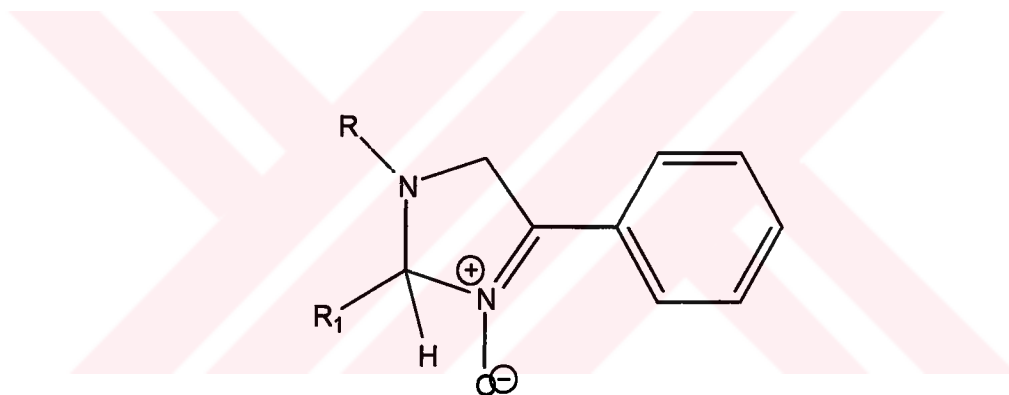


Figure 1.3 Chemical Diagram of Compounds 1 with groups that can be substituted various functional structures.

In our study, X-ray data for the crystal structures are collected with Enraf Nonius CAD-4 diffractometer that is at X-Ray Laboratory, Department of Physics Engineering, Faculty of Engineering, Hacettepe University. After this, the collected data are solved by direct methods with SHELXS-97 (Sheldrick, 1998) program and the atomic parameters are refined by least squares and difference-Fourier method with SHELXL-97 (Sheldrick, 1998) program at Department of Physics, Faculty of Arts & Sciences, Dokuz Eylül University. In different steps of the study for geometrical calculations and molecular graphics; WINGX (Farrugia, 1999),

ORTEP3 (Farrugia, 1997), PLATON (Spek, 1990), PLUTON (Spek, 1990; Motherwell & Cleegg, 1978) package programs were used.

Conformational study about the molecule was performed by using AM1 and PM3 semi-empirical molecular orbital methods, which is greatly convenient with experimental results, via HyperChem 6.0 package program (HyperCube Inc., 1996) on the Intel Pentium II computer.



CHAPTER TWO

X-RAY DIFFRACTION DATA

2.1 Measurement Methods of Diffraction Intensities

In this study, the data were collected with an Enraf-Nonius CAD-4 diffractometer. A single crystal diffractometer consists of an X-ray source, an X-ray detector, a goniometer that orients the crystal so that a chosen X-ray diffracted beam can be received by the detector, and a computer that controls (Enraf-Nonius, 1993) the goniometer and detector movements and performs the mathematical operations required to position the crystal and the detector in the desired orientations (Giacovazzo et al, 1998).

There are three well-known methods for measurement of diffraction intensity. In first of these, both crystal and detector are not moved. While crystal is constant at the reflection position, detector is constant at the 2θ position and intensity measured.

In the “ w -scan” mode, the detector is held at the 2θ angle of the actual reflection and the crystal rotated on the w -axis of the diffractometer.

In the “ $w/2\theta$ -scan” mode, both crystal and detector are moved. The crystal is rotated by Δw , while the detector is rotated in the 2θ -circle by an angular velocity, which is twice of the crystal rotation.

The principles of “ w -scan” and “ $w/2\theta$ -scan” methods are shown in Figure 2.1(a) and 2.1(b), respectively.

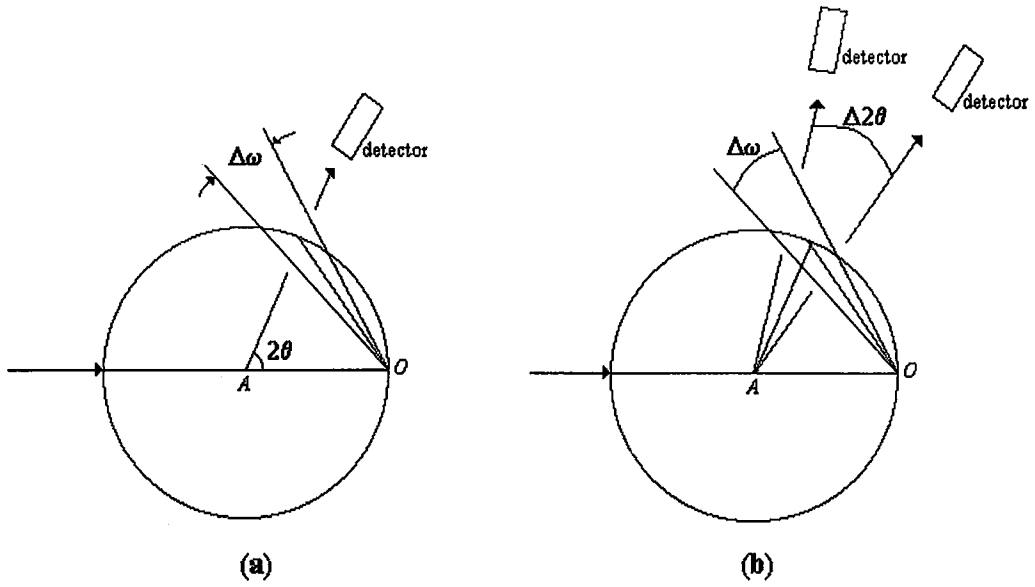


Figure 2.1 Diffraction scan types. (a) ω -scan (b) $\omega/2\theta$ -scan

2.2 Scattering of X-rays by a Crystal

An Argand diagram may represent the combination of waves. The waves are represented as vectors with real and imaginary components. We consider that the X-rays diffracted by structure with N atoms. The resultant of N waves is,

$$\vec{F} = f_1 e^{i\phi_1} + f_2 e^{i\phi_2} + \dots + f_j e^{i\phi_j} + \dots + f_N e^{i\phi_N} \quad (2.1)$$

$$\vec{F} = \sum_{j=1}^N f_j e^{i\phi_j} \quad (2.2)$$

On an Argand diagram, (2.2) expresses a polygon of vectors (Figure 2.2); the resultant \vec{F} is given by

$$\vec{F} = |F| e^{i\phi} \quad (2.3)$$

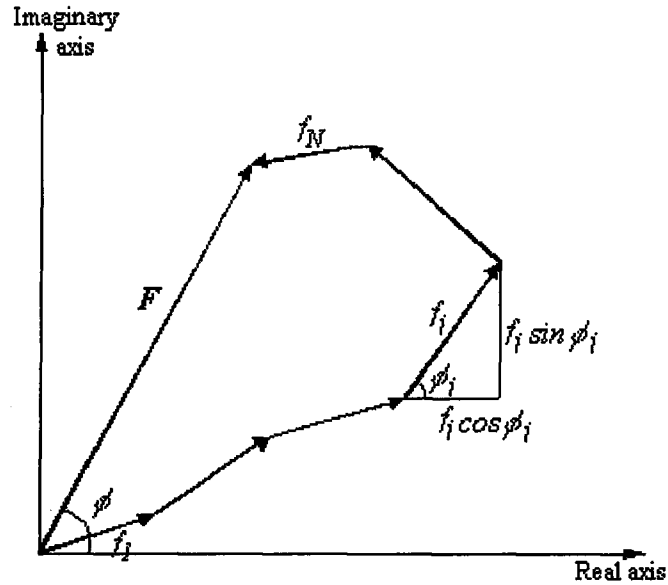


Figure 2.2 Combination of N waves on an Argand diagram.

The amplitude $|F|$ is given by

$$|F|^2 = \vec{F}\vec{F}^* \quad (2.4)$$

where \vec{F}^* is the complex conjugate of \vec{F} :

$$\vec{F}^* = |F|e^{-i\phi} \quad (2.5)$$

By analogy we can write,

$$|F| = (A^2 + B^2)^{1/2} \quad (2.6)$$

where

$$A = \sum_{j=1}^N f_j \cos \phi_j \quad \text{and} \quad B = \sum_{j=1}^N f_j \sin \phi_j \quad (2.7)$$

A and B are, respectively, the real and imaginary components of \vec{F} , and the phase angle ϕ is given by

$$\tan \phi = \frac{B}{A} \quad (2.8)$$

In unit cell if we consider a structure, which has fractional coordinates x_j, y_j, z_j ($j=1, 2, \dots, N$), the resultant of the path difference of the waves, which are scattered by j .th atom, is as follows

$$\delta_j = \lambda(hx_j + ky_j + lz_j) \quad (2.9)$$

The phase difference can be written as

$$\Phi_j = \left(\frac{2\pi}{\lambda}\right)\delta_j \quad \text{or} \quad \Phi_j = 2\pi(hx_j + ky_j + lz_j) \quad (2.10)$$

2.3 Crystal Structure Factor

In (2.1), F is called structure factor. The term structure factor is used to represent the scattering by the contents of one unit cell of a structure.

If we add (2.10) into (2.2); we can write

$$F_{hkl} = \sum_{j=1}^N f_j \exp[2\pi i(hx_j + ky_j + lz_j)] \quad (2.11)$$

for structure factor.

In order to evaluate the F_{hkl} , we need also f_j , called the atomic scattering factors. If we know their values, the calculation of atomic scattering factors are complicated. Because; they are tabulated as functions of $\frac{\sin \theta}{\lambda}$, and denoted as f_j . The atomic scattering factor depends upon the nature of the atom. f_j depends upon the number of extra nuclear electrons in the atom: its maximum value for a given atom j is Z_j , the atomic number of the j .th atomic species. (Ladd & Palmer, 1988).

The variation of f_j with $\frac{\sin \theta}{\lambda}$ is shown in Figure 2.3.

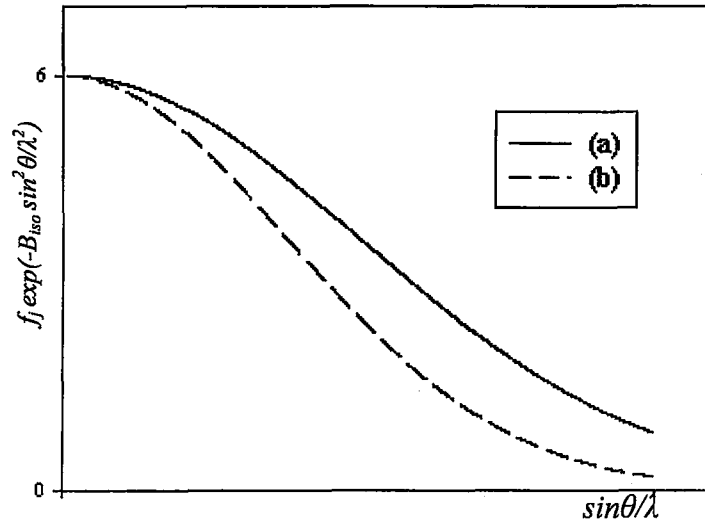


Figure 2.3 Atomic scattering factors: (a) stationary atom, (b) atom corrected for thermal vibration.

2.4 Fourier Synthesis and Electron Density

Electron's distribution around the atoms is presented electron density function. Because of three dimension periodicity's of the lattice, the electron density at the point (x, y, z) as $\rho(x, y, z)$ can be represented as a triple Fourier series. Then we may write

$$\rho(x, y, z) = \frac{1}{V} \sum_h \sum_k \sum_l F_{hkl} \exp[-2\pi i(hx + ky + lz)] \quad (2.12)$$

where V and F_{hkl} are the unit-cell volume and the structure factor, respectively. From (2.3) we can write

$$\Phi_{hkl} = \arctan \left[\frac{B_{hkl}}{A_{hkl}} \right] \quad (2.13)$$

where Φ_{hkl} is phase angle of crystal structure factor. From Friedel's law, which says, the diffraction patterns have a center of symmetry,

$$F_{hkl} = F_{\bar{h}\bar{k}\bar{l}} \quad \text{or} \quad \Phi_{hkl} = \Phi_{\bar{h}\bar{k}\bar{l}} \quad (2.14)$$

if we unite (2.3) and (2.12) the electron density function can be written as

$$\rho(x, y, z) = \frac{1}{V} \sum_h \sum_k^{+\infty} \sum_l^{-\infty} F_{hkl} \exp[2\pi i(hx + ky + lz) + \Phi_{hkl}] \quad (2.15)$$

If we write this equation as trigonometric functions, the electron density function is given as follows

$$\rho(x, y, z) = \frac{1}{V} \sum_h \sum_k^{+\infty} \sum_l^{-\infty} |F_{hkl}| \cos[2\pi(hx + ky + lz) - \Phi_{hkl}] \quad (2.16)$$

As we can see from (3.16), if we know the structure factors, F_{hkl} , the electron densities can be calculated. The peaks at the electron density maps can be used for determining the atom's positions. The experimental measured diffraction intensity give the amplitude of crystal structure factors.

But we need the phases, Φ_{hkl} , for three dimensional electron density map. In this study, "direct methods" has been used in order to derive the phases.

2.5 Data Reduction

The general process of converting electronic measurements into feasible diffraction data is called "data reduction". For each intensity maxima, data reduction includes an integration of the peak including corrections for the spot shape, subtraction of the relative background intensity, corrections for the geometry of the instrument, corrections for crystal decay, and averaging or merging of equivalent data.

The first step involves both an integration of the peak and a subtraction of the background. The integration step must include corrections for overly strong peaks that have been recollected at shorter times or with attenuators. This step sometimes includes corrections for the shape of the diffraction spot. The background, that is presumed to run beneath the peak measurement, is measured both before and after the peak or is sampled in various areas around the peak. Background scattering may

be due to scattering from the sample mount, scattering from air, fluorescence radiation from the sample or mount, and cosmic radiation. This step produces both crude intensity and estimates of the standard uncertainties, often called estimated standard deviations, in the intensity. The standard uncertainties that calculated directly from counting statistics were found to be underestimates of the true uncertainties. Now standard uncertainties in intensity include a small "instrument instability" correction term. The following expression is usually applied in calculating structure factor amplitudes.

$$I_{hkl} = K.L.p.T.A.E.|F_{hkl}|^2 \quad (2.17)$$

In this equation, the symbols indicate;

K: scale factor

L: Lorentz factor

p: Polarization factor

T: Debye-Waller Temperature factor

A: Absorption factor

E: Extinction factor

To use in crystal structure analysis, diffraction intensity that are measured must be corrected by these factors so that F_{hkl} values are gained.

2.5.1 Lorentz Correction

Some peaks, such as those peaks near to the rotation axis, spend more time passing through the Ewald sphere of reflection than do others. This difference in time is corrected by a term called the Lorentz factor. For point detector systems performing ω - 2θ or ω scan, this correction is simply

$$L = \frac{1}{(\sin 2\theta)} \quad (2.18)$$

Area detector intensity are generally not located in the horizontal plane, so different formulas are used that is based upon whether the data are being collected using ω or f scans.

2.5.2 Polarization Correction

At different scattering angles the scattered beam will be attenuated by the polarization of the beam by the sample. If the incident radiation is plane polarized (random orientation of the electric vector of the radiation) then the polarization correction is given by

$$p = \frac{1}{2} (1 + \cos^2 2\theta) \quad (2.19)$$

If a monochromator is inserted in the incident beam, then the X-rays impinging on the sample are already partially polarized from the monochromator crystal and a different formula is used that depends upon the geometry of the monochromator.

2.5.3 Absorption Correction

The absorption of X-rays follows Beer's Law:

$$I = I_0 \exp(-\mu x) \quad (2.20)$$

where I is transmitted intensity, I_0 is incident intensity, x is thickness of material, μ is linear absorption coefficient of the material. The linear absorption coefficient depends on the substance, its density, and the wavelength of radiation. Since μ depends on the density of the absorbing material, it is usually tabulated as the mass absorption coefficient $\mu_m = \left(\frac{\mu}{\rho}\right)$. The linear absorption coefficient is then calculated from the formula:

$$\mu = \rho \left(\frac{P_n}{100} \right) \left(\frac{\mu}{\rho} \right)_n \quad (2.21)$$

where the summation is carried out over the n atom types in the cell, P_n is the percent by mass of the given atom type in the cell and ρ is the density of the crystal. The absorption coefficients for crystals in this study are found 0.0105 mm^{-1} for $C_{29}H_{25}N_3O_3$ from Table 2.1. How to reduce crude X-ray diffraction intensity from diffractometer was elaborately reported by Kopfmann and Huber (Kopfmann & Huber, 1968).

Table 2.1 Atomic mass and mass absorption coefficients for $C_{29}H_{25}N_3O_3$.

Atom	Number of atoms	Atomic mass m (a.m.u.)	Total mass (a.m.u.)	Percentage (%) P_n	Mass absorption coefficient (MoK $_{\alpha}$) (cm^2/g)
C	29	12.01	348.29	75.14	0.70
H	25	1.01	25.25	5.44	0.37
N	3	14.01	42.03	9.07	1.10
O	3	15.99	47.97	10.35	1.50

Absorption of X-rays by the sample is often the most difficult correction to perform. The extent of absorption depends on the size and shape of the crystal as well as the types and relative amounts of different atoms in the sample, and the wavelength of radiation used in the experiment. Also absorption from the sample mount may need to be included in the correction. Most researchers try to reduce the effects of absorption by reshaping the sample, properly mounting the sample, using a smaller crystal, or by using a higher energy radiation. There are four general classes of absorption corrections, analytical, empirical, geometrical, and Fourier.

2.5.4 Debye-Waller Temperature Factor Correction

Thermal motion affects X-rays intensity. Normal scattering factor curves are calculated through the electron distribution that belongs to a fix atom. But, in fact, atoms in the crystal vibrate continuously around their points. The magnitude of vibration depends on temperature, atom's mass and interaction forces, which are taken place by perimeter atoms. Vibration is usually so high at high temperatures. Thermal motion causes that electron cloud is located into larger volume and this case causes that scattering power of real atom decreases rapidly (Figure 2.3). The variation of scattering power can be written as

$$\exp\left(-B \frac{\sin^2 \theta}{\lambda^2}\right) \quad (2.22)$$

where B is isotropic temperature factor and is proportional to the average of atomic vibration amplitude's square ($\overline{u^2}$) (Aygün, 1997).

$$B = 8\pi^2 \overline{u^2} \quad (2.23)$$

so, scattering factor for a real atom as follows

$$f = f_o \exp\left(-B \frac{\sin^2 \theta}{\lambda^2}\right) \quad (2.24)$$

where f_o is scattering amplitude at 0 K and f is scattering factor at laboratory temperature. After the Lorentz-polarization ($L-p$) correction is done, observed average intensity becomes

$$\overline{I_{obs}} = \left\langle |F_{obs}|^2 \right\rangle_{ave} \quad (2.25)$$

Theoretical average intensity for a structure with N atoms in the unit-cell is

$$\overline{I_{cal}} = \sum_{i=1}^N f_i^2 \quad (2.26)$$

If we unite (2.25) and (2.26),

$$\overline{I_{obs}} = \sum_{i=1}^N f_{oi}^2 \exp\left(-B \frac{\sin^2 \theta}{\lambda^2}\right) \quad (2.27)$$

here B is constant for all atoms and can be calculated. Than, we can write

$$\overline{I_{obs}} = \exp\left(-B \frac{\sin^2 \theta}{\lambda^2}\right) \sum_{i=1}^N f_{oi}^2 \quad (2.28)$$

In addition,

$$\overline{I_{cal}} = C \overline{I_{obs}} \quad (2.29)$$

$$\overline{I_{cal}} = C \exp\left(-B \frac{\sin^2 \theta}{\lambda^2}\right) \sum_{i=1}^N f_{oi}^2 \quad (2.30)$$

$$\ln \left[\frac{\overline{I_{cal}}}{\sum_{i=1}^N f_{oi}^2} \right] = \ln C - \left[2B \frac{\sin^2 \theta}{\lambda^2} \right] \quad (2.31)$$

The variation of $\ln \left[\frac{\overline{I_{cal}}}{\sum_{i=1}^N f_{oi}^2} \right]$ with $\frac{\sin^2 \theta}{\lambda^2}$ is shown in Figure 2.4. So we can find

the isotropic temperature factor, B , from the slop of the graphic.

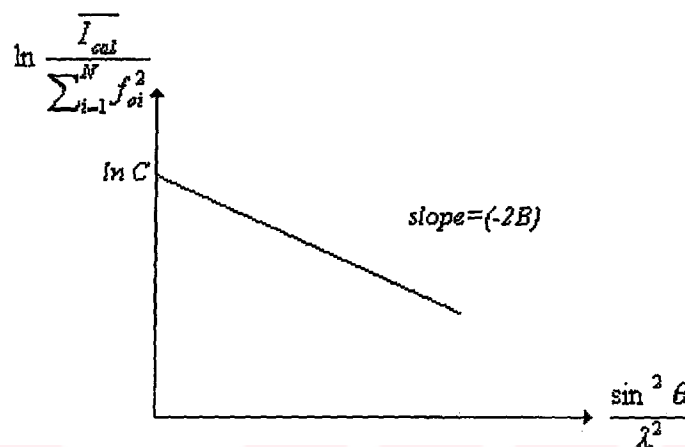


Figure 2.4 Wilson plot.

Here C depends on k that is scale constant between $|F_{obs}|$ and $|F_{cal}|$, and can be written as

$$k = \frac{1}{\sqrt{C}} \quad \text{or} \quad |F_{obs}| = k|F_{cal}| \quad (2.32)$$

2.5.5 Extinction Correction

The extinction correction, E , is not automatically applied although the program will often prompt when one might be necessary. Real crystals can be envisaged as a mosaic of crystalline blocks, each block tilted very slightly with respect to the others and separated by cracks and faults. When an X-ray beam is diffracted by underlying blocks; thus the underlying blocks contribute less than expected to the overall effect. The above manifestation of extinction can be detected when $|F_{obs}|$ is less than $|F_{cal}|$, particularly for very intense reflections. The correction then involves rescaling to wake the most intense Bragg reflections agree with those calculated.

2.5.6 Anomalous Scattering Factor

In discussing the scattering of X-rays by atoms, we have implicitly assumed that the frequency of the radiation used was far from that corresponding to any electronic transition in the atoms being irradiated. But when this condition does not hold, the scattering factor for that atom is no longer a scalar, but rather becomes a complex. This situation is called “anomalous scattering” or “anomalous dispersion”. If we write an expression for scattering factor:

$$f = f_o + \Delta f' + i\Delta f'' \quad (2.33)$$

where $\Delta f'$ is a real correction, usually negative, and $\Delta f''$ is imaginary component respect to f_o and $\Delta f'$. A possible situation is illustrated for normal case in Figure 2.5 (a) and for anomalous case in Figure 2.5 (b).

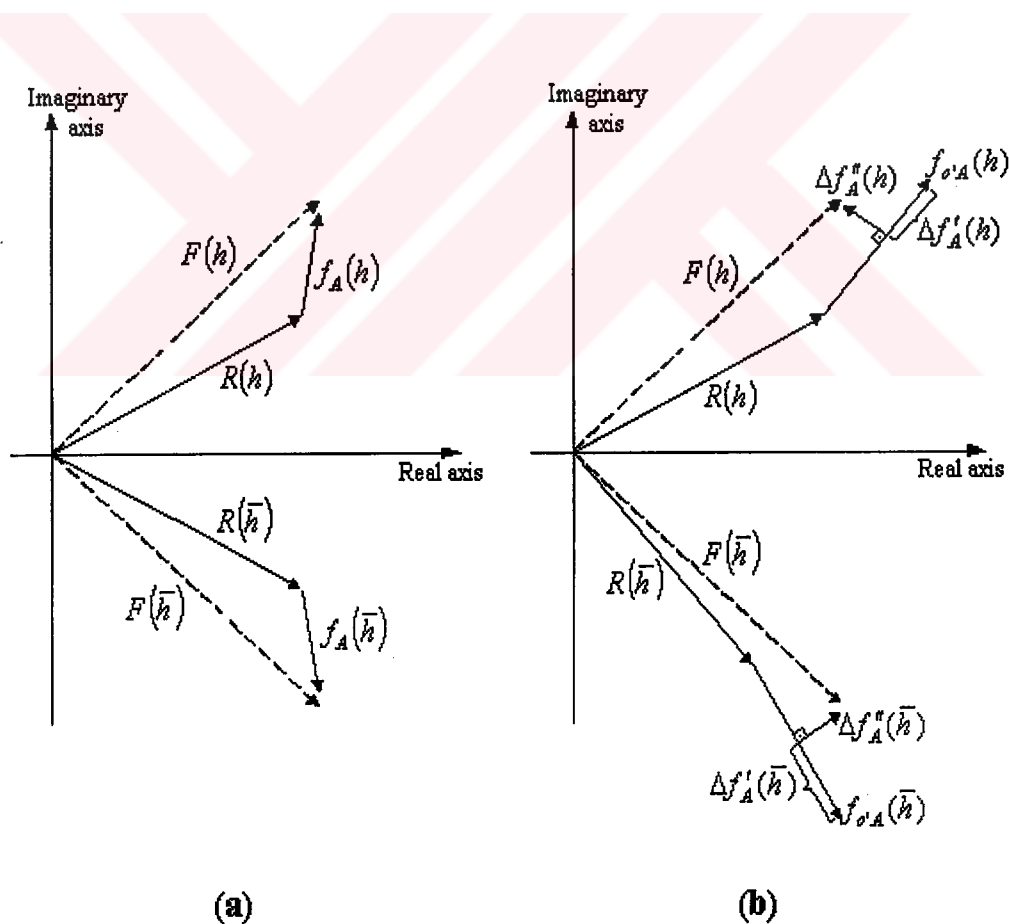


Figure 2.5 Anomalous scattering of atom A with respect to the rest of the structure

R: (a) normal case- $|F(h)| = |F(\bar{h})|$; (b) anomalous case- $|F(h)| \neq |F(\bar{h})|$.

CHAPTER THREE

SOLUTION OF CRYSTAL STRUCTURE

3.1 Introduction

The success-controlling step of a structure determination is normally the step of finding the correct locations for the first atoms of the model structure: once model is launched, the techniques for adding atoms to trial structure (Fourier techniques) and refining the structure (least-square or Fourier methods) are more straightforward procedures.

The number of techniques used for the initiation of a small molecule model is not large.

3.2 The Phase Problem

There are several ways of describing the phase problem of crystallography:

Both the phases and the magnitudes of the Bragg reflections must be known to form the image of the scattering material, but only the magnitudes are observed.

It's a Catch-22 situation: atom positions can be calculated if phase information is known, and phase information can be calculated if atom positions are known.

The phase problem makes the structure determination experiment become an indirect process of modelling the crystal; if the reflection intensity of the model match the measured values the model is assumed correct.

The phase problem is what makes crystallography fun: it puts an element of 'puzzle solving' into the structure determination experiment.

In the structure determination experiment the phase problem makes the major hurdle that of getting the model structure started: the problem of how to use the large amount of experimental data obtained to begin deducing the atom arrangements which produce those data.

If the structure is centrosymmetric with the origin at the center of symmetry, the phase angle, Φ_{hkl} , for each reflection must be 0° or 180° . Thus

$$F_{hkl} = |F_{hkl}| \cos(\Phi_{hkl}) = \pm |F_{hkl}| \quad (3.1)$$

and the phase problem becomes the problem of determining the correct sign for each of the thousands of structure factor amplitudes that were measured. For n unique reflections, the number of combinations of phases possible are 2^n (Gökçe, 2002)

If the structure is not centrosymmetric the phase angle can have any value ranging over an entire circle. Assuming the phase angles need to be known within $\pm 45^\circ$ in order to get a sufficiently good image of the structure. The number of possible phase angle combinations becomes 4^n (Gökçe, 2002).

Reflection intensity is the focus of the front end of the structure determination experiment (data collection) and the F or F^2 values are the focus of the later part of the experiment (least-squares refinement). With this emphasis on reflection amplitude it is important to note that the phase information can be more important than the amplitude data for the determination of the structure (Lecture Notes, 2001, pp.XV-1).

3.3 The trial-and-error method

This method was about the only approach available in the 1920's and 1930's. One part of the research was to find crystals, which had most, or all, of the atoms located in special positions of highly symmetric space groups. In this way the choices for the atom positions were limited. The description by Linus Pauling of the structural research done in 1920's at Cal Tech provides interesting insights into this era of crystallography.

3.4 The Patterson Technique

This technique was the dominant method used in structure determination research from the mid-1930's until the mid-1960's. This approach, which is still in use, requires no phase information and uses all of the reflection data. The method involves the unraveling of a map of inter-atomic vectors to determine the atom arrangement, which produced the vector pattern. A Patterson map contains too many vectors to unscramble if the number of unique atoms is greater than about 20, unless one or more of the atoms are significantly heavier than the others. In this case the vectors involving the heavy atoms dominate the vector map and can be used to locate the heavy atoms in the unit-cell.

The last method that took place in 1960's and 1970's, and has been used in this study, "direct methods", will be discussed at length in a following sections.

3.5 Direct Methods

Up to the early sixties, the principal method used for structure determination was by interpretation of the Patterson function. But this method could not apply to determine structure of so-called light atoms compounds by chemists. For this reason, chemists needed to its derivatives substituted by using heavy atoms such as bromine, iodine or halogenated derivatives. The development of the so-called "Direct Methods" of phase determination has removed this limitation.

The name “Direct Methods” is derived from the fact that the phases of the structure factors are derived from the magnitudes of the F 's rather than indirectly by an interpretation of the Patterson function. A short and not too detailed representation of principles of Direct Methods was presented in the next section.

3.5.1 Normalized Structure Factors and Intensity Statistics

Some structure factors that correspond to a net scattering from a few atoms more or less in phase, so that $|F_{hkl}|$ is a non-negligible fraction of what it would be if many atoms scattered in phase. There is always a certain proportion of such reflections in any structure, but it is not usually obvious which reflections these are, because of the rapid decline in atomic scattering power (for X-rays) with increasing scattering angle and with temperature. However, correction for these to effects is straightforward, and is the essential step in the calculation of normalized structure factor magnitudes ($|E_{hkl}|$), which represent the ratio of the $|F_{hkl}|$ to its expectation value at the $\sin\theta/\lambda$ for that hkl . Each $|F_{hkl}|$ is converted to the corresponding $|E_{hkl}|$ by dividing by r. m. s. value of the atomic scattering factors in the structure, at the value of $\sin\theta/\lambda$ corresponding to that hkl , and by the average temperature factor for the atoms in the structure:

$$E_{hkl} = \frac{|F_{hkl}|}{\Sigma} \quad (3.2)$$

where $\Sigma = \sqrt{\varepsilon \sum_j f_j^2 \exp\left[-B \frac{\sin^2 \theta}{\lambda^2}\right]}$, with B an average isotropic temperature factor (Lecture Notes, 2001, pp.XV-1).

Central Limit Theorem states that the distribution of a sum of n independent random variables tends, as n goes to infinity, to abnormal or Gaussian distribution function. The normal or Gaussian distribution function is given by

$$p(x) = \frac{1}{\sigma\sqrt{2\pi}} \exp\left[\frac{-(x-m)^2}{2\sigma^2}\right] \quad (3.3)$$

where m is the mean and σ is the standard deviation.

If the atoms in a crystal are considered to be arranged randomly, and the number of atoms is large, the Central Limit Theorem can be applied to the distribution of the intensity of diffraction from the crystal, since that intensity depends on F_{hkl}^2 , and F_{hkl} is just the sum of the scattering from many randomly distributed atoms. When the calculation is made for $|E_{hkl}|$ values instead of $|F_{hkl}|$'s, the results are particularly simple, since the distribution of $|E_{hkl}|$ is Gaussian. Table 4.1 presents some useful results for the equal-atom case (Luger, 1980, pp.214).

Table 3.1 Some statistical properties of normalized structure factor magnitudes*.

	Non-centrosymmetric	Centrosymmetric	Hypercentric [#]
$\langle E \rangle$	0.886	0.798	0.718
$\langle E ^2 \rangle$	1.000	1.000	1.000
$\langle E^2 - 1 \rangle$	0.736	0.968	1.145

* The symbol $\langle \rangle$ represents an average overall hkl .

[#] The hypercentric distribution applies to structures containing centrosymmetric molecules that lie in general positions in centrosymmetric space groups.

3.5.2 Fundamental Formulae

The principles of direct methods are based on the fact that the experimental data, that is the magnitude of structure factors. This was first pointed out by Harker-Kasper inequalities (Harker & Kasper, 1948).

By application of the Cauchy-Schwarz inequality

$$\left| \int f(x)g(x)dx \right|^2 \leq \left(\int |f(x)|^2 dx \right) \left(\int |g(x)|^2 dx \right) \quad (3.4)$$

to the expression for the structure factor, some remarkable results can be obtained. With

$$F(\vec{h}) = \int_V \rho(\vec{r}) e^{2\pi i \vec{h} \cdot \vec{r}} dV \quad (3.5)$$

supposing $\rho(\vec{r}) \geq 0$ for all \vec{r} , and

$$f(\vec{h}) = \rho(\vec{r})^{1/2} \quad (3.6)$$

$$g(\vec{h}) = \rho(\vec{r})^{1/2} e^{2\pi i \vec{h} \cdot \vec{r}} \quad (3.7)$$

where $\vec{h} \equiv (h, k, l)$. We get

$$|F(\vec{h})|^2 \leq \left(\int_V \rho(\vec{r}) dV \right) \left(\int_V \rho(\vec{r}) |e^{2\pi i \vec{h} \cdot \vec{r}}|^2 dV \right) \quad (3.8)$$

Since

$$|e^{2\pi i \vec{h} \cdot \vec{r}}|^2 = 1 \quad (3.9)$$

and

$$\int \rho(\vec{r}) dV = Z \quad (3.10)$$

with $F(000)$ being equal to the number of electrons in the unit cell, we get

$$|F(\vec{h})| \leq F(000) \quad (3.11)$$

which is, of course, a trivial result. However, with the additional provision of special symmetry elements present in the unit cell, some important non-trivial results can be derived. Let us assume, for example, that an inversion centre is present. Then $F(\vec{h})$ reduces to

$$F(\vec{h}) = \int_{V/2} \rho(\vec{r}) \left(e^{2\pi i \vec{h} \cdot \vec{r}} + e^{-2\pi i \vec{h} \cdot \vec{r}} \right) dV = 2 \int_{V/2} \rho(\vec{r}) \cos(2\pi \vec{h} \cdot \vec{r}) dV \quad (3.12)$$

Choosing f and g as above, we get

$$|F(\vec{h})|^2 \leq 2Z \int_{V/2} \rho(\vec{r}) (\cos(2\pi \vec{h} \cdot \vec{r}))^2 dV \quad (3.13)$$

with $\cos^2 \alpha = \frac{1}{2}(1 + \cos 2\alpha)$ we get

$$F(\vec{h}) \leq 2Z \left(\int_{V/2} (\rho/2) dV + \int_{V/2} (\rho/2) \cos(2\pi 2\vec{h} \cdot \vec{r}) dV \right) = \frac{Z}{2} (Z + F(2\vec{h}))$$

or with $Z = F(000)$,

$$|F(\vec{h})| \leq F(000) \left(F(000)/2 + F(2\vec{h})/2 \right) \quad (3.14)$$

Defining

$$u(\vec{h}) = \frac{F(\vec{h})}{F(000)} \quad (3.15)$$

we get finally

$$|u(\vec{h})| = \frac{1}{2} (1 + u(2\vec{h})) \quad (3.16)$$

and with using u instead of (3.14) reduces to $|u(\vec{h})| \leq 1$.

From (3.16) information about a phase, or, since we have a centrosymmetric problem, about a sign, can be derived from the magnitude of u 's and the $|u|$'s are derive directly from the experimental data. Equation (3.16) is only used for strong reflections. This is a limitation in direct methods due to the fact that suitable reflections are usually rare, for instance 10%. Therefore, Harker-Kasper inequality is no longer applied in practical structure analysis (Harker & Kasper, 1948; Gillis, 1948; Goedkoop, 1950; MacGillavry, 1950). A large number of investigations on that subject have been initiated, of which one of the earlier important results was the Sayre equation developed in 1952 (Sayre, 1952). It is one of the basic formulae of "Direct Methods".

A simple derivation of Sayre's equation can be obtained using a simplified structural model. Let us use point-shaped atoms of unique density having no thermal motion, so that there is no overlap between pairs of atoms. For this model, let us assume that $\rho(\vec{r}) = [\rho(\vec{r})]^2$.

The Fourier transform of $\rho(\vec{r})$ is then denoted by $F(\vec{h})$. Since transform of a product can be expressed by a convolution operation (Convolution theorem), we get

$$\Gamma(\rho(\vec{r})) = \{\Gamma[\rho(\vec{r})]\}^2 \quad (3.17)$$

or, using $F(\vec{h})$ for the Fourier transform,

$$F(\vec{h}) = \int_{V'} F(\vec{h}') F(\vec{h} - \vec{h}') dV'. \quad (3.18)$$

Since normalized E- values are closely related to that model, and since for a single crystals the integral the integral over the reciprocal lattice can be replaced a sum, we get

$$E(\vec{h}) = T \sum_{\vec{h}'} E(\vec{h}') E(\vec{h} - \vec{h}'). \quad (3.19)$$

(3.19) is the Sayre equation, which is a key formula in the theory of “Direct Methods”. The non-negative factor T does not affect its application, since it can be calculated. Although we have derived this equation from a very special model, it is valid generally. For a real structural model, only another factor T has to be introduced. From Sayre’s equation, two formulae to be applied in actual phase determination will be derived, depending on whether the structure is centrosymmetric or acentric.

It must be noted at this point that the procedure in practical direct phase determination is different in the centric and acentric case. This is because the centric structure factors have phases restricted to 0 or π . Since it is, in general, less difficult to decide between two possible values than to determine a phase out of the whole range from 0 to 2π , it has become customary, although not necessary, to handle these two cases separately. If it could not be decided unambiguously by space group determination whether a center of symmetry is present or not, the distribution and the averages of E-values can be used as further criteria (Dunitz, 1979).

In the centrosymmetric case, the E values have a sign of + or -. Sayre’s equation can then be interpreted as follows. For reflections \vec{h} with $|E(\vec{h})|$ being sufficiently large, it is likely that the sum on the right side of (3.19) will contain more terms $E(\vec{h}') E(\vec{h} - \vec{h}')$ having the same as sign as $E(\vec{h})$ itself, than terms of opposite sign. Otherwise equation (3.19) could not hold. This is especially true for those terms for which $|E(\vec{h}')|$ and $|E(\vec{h} - \vec{h}')|$ are large, since they are the major contributors to the sum. So there exists a more than 50% probability that for large E-values.

$$s(\vec{h}) = s(\vec{h}')s(\vec{h} - \vec{h}') \quad (3.20)$$

where $s(\vec{h})$ denotes the sign of $E(\vec{h})$. This equation remains valid if on the left side \vec{h} is replaced by $-\vec{h}$, since $s(\vec{h}) = s(-\vec{h})$. Setting $-\vec{h} = \vec{h}_1$, $\vec{h}' = \vec{h}_2$ and $\vec{h} - \vec{h}' = \vec{h}_3$, we get finally

$$s(\vec{h}_1) = s(\vec{h}_2)s(\vec{h}_3) \quad (3.21)$$

or

$$s(\vec{h}_1)s(\vec{h}_2)s(\vec{h}_3) = 1 \quad (3.22)$$

if the reflections \vec{h}_1 , \vec{h}_2 , \vec{h}_3 satisfy the equation

$$\vec{h}_1 + \vec{h}_2 + \vec{h}_3 = 0 \quad (3.23)$$

Reflection triplets for which (3.23) holds are said to be related by a Σ_2 relation. As we shall see, these Σ_2 play an important role with all applications of direct methods.

From the derivation of (3.22), it is clear that this equation cannot hold exactly, so that instead of writing “=” it would be better to write “ \approx ”. Fortunately, the probability that (3.22) is valid for a given structure can be calculated, as was first done by Cochran and Woolfson (Woolfson, 1954; Cochran & Woolfson, 1955; Cochran, 1952; Cochran, 1953; Cochran, 1954; Cochran, 1955; Zachariasen, 1952). The probability in question under some approaches can be expressed by

$$p = \frac{1}{2} + \frac{1}{2} \tanh \left(\frac{1}{\sqrt{N}} |E(\vec{h}_1)E(\vec{h}_2)E(\vec{h}_3)| \right) \quad (3.24)$$

where N denotes total number of atoms in the unit cell.

Now we can interpret the sign relationship (3.22) together with (3.24) as follows. If we have three reflections connected by a Σ_2 relation (3.23), and if the signs of two of them are known, then the sign of the third reflection can be inferred from (3.22) with a probability given by (3.24). This probability increases with the magnitudes of contributing E 's, but decreases with the number of atoms in the unit cell, thus with size of the structure, as shown by (3.24). Several problems arise with this interpretation of (3.22). The first is, where to obtain the known signs so that the sign relationship can be applied? To overcome this problem appropriate starting set of

phase is chosen from strong reflections and using known phases belonged to strong reflections starting set is gradually expanded till all reflection regardless of their intensity were included. Another question is, are the probabilities calculated from (3.24) large enough so that sign determinations from (3.22) valid? To get an impression of the magnitude of p , we have calculated p from (3.24) for various values of N and for different magnitudes of E , assuming $|E(\vec{h}_1)| = |E(\vec{h}_2)| = |E(\vec{h}_3)| = E$. The results were given in Table 3.2.

Table 3.2 Probabilities for the sign relationship calculated for various parameters E and N .

E	$N = 40$	80	120	160	200
3.0	1.00	1.00	0.99	0.99	0.98
2.0	0.93	0.86	0.81	0.78	0.76
1.0	0.58	0.55	0.54	0.54	0.53

If, in the latter stages of sign determination, a large number of signs is known, it can happen that an unknown reflection is contained in more than one Σ_2 relation. Then, of course,

$$s(\vec{h}) = \sum_{\vec{h}'} s(\vec{h}') s(\vec{h} - \vec{h}') \quad (3.25)$$

is a better approximation of Sayre's equation, and in this case probability for the sign of \vec{h} to be "+" is given by

$$p_+(\vec{h}) = \frac{1}{2} + \frac{1}{2} \tanh\left(\frac{1}{\sqrt{N}} |E(\vec{h})| \sum_{\vec{h}'} E(\vec{h}') E(\vec{h} - \vec{h}')\right) \quad (3.26)$$

while the probability $p_-(\vec{h})$ of a sign to be "-" is given by

$$p_-(\vec{h}) = 1 - p_+(\vec{h}) \quad (3.27)$$

For the phase determination in the acentric case, a further formula can be derived from Sayre's equation. Separating (3.19) into its real and imaginary part, we get

$$\left|E(\vec{h})\right| \sin \varphi(\vec{h}) = T \sum_{\vec{h}'} \left|E(\vec{h}')E(\vec{h} - \vec{h}')\right| \sin(\varphi(\vec{h}') + \varphi(\vec{h} - \vec{h}')) \quad (3.28)$$

and

$$\left|E(\vec{h})\right| \cos \varphi(\vec{h}) = T \sum_{\vec{h}'} \left|E(\vec{h}')E(\vec{h} - \vec{h}')\right| \cos(\varphi(\vec{h}') + \varphi(\vec{h} - \vec{h}')) \quad (3.29)$$

By division, we get

$$\tan \varphi(\vec{h}) = \frac{\sum_{\vec{h}'} \left|E(\vec{h}')E(\vec{h} - \vec{h}')\right| \sin(\varphi(\vec{h}') + \varphi(\vec{h} - \vec{h}'))}{\sum_{\vec{h}'} \left|E(\vec{h}')E(\vec{h} - \vec{h}')\right| \cos(\varphi(\vec{h}') + \varphi(\vec{h} - \vec{h}'))} \quad (3.30)$$

This is the well-known “tangent formula” derived by Karle and Hauptman (Hauptman & Karle, 1956; Karle & Hauptman, 1950; Karle & Hauptman, 1956; Karle & Hauptman*, 1956; Karle & Hauptman, 1961). Just as (3.22) is the key formula for phase determination in the centric case, the tangent formula is the key formula for phase determination in the acentric case.

3.6 Criteria of Correctness Set of Phases

Phase determination has usually given more than one solution. For a few sets of given phases, calculating and interpreting of electron density maps that help to perceive right structure corresponding to these sets of phase have a long time. Instead of, this computing some of appropriate functions which are referred to as criteria of correctness set of phases or “figures of merit” (FOM) is easier than other ways. FOM, makes possible the fact that correctness of each sets of phase is precedingly estimated. Some of the FOMs are MABS, NQUAL, R_{α} , CPHASE, ψ_0 , ... Let us investigate prevalently used of them.

3.6.1 MABS

It is defined as

$$MABS = \frac{\sum_h \alpha_h}{\sum_h \langle \alpha_h \rangle} = \frac{A}{A_e} \quad (3.31)$$

which triplet relations studied in estimation of phase are connected with dependence among relations in question. In order to obtain correct structure, A_e that is theoretically estimated and A close on each other and MABS is approximately equal to 1. In practice, for approaching to right phase set A must be bigger than A_e and values of MABS must be ranging from 0.9 to 1.3.

3.6.2 NQUAL

It is defined as

$$NQUAL = \frac{\sum [\sum (E_1 E_2) \sum (E_3 E_4 E_5)]}{\sum [\sum (E_1 E_2) \|\sum (E_3 E_4 E_5)\|]} \quad (3.32)$$

For right structure solution, the value of NQUAL must be close to -1 . For random phases, it is equal to zero.

3.6.3 R_α FOM

It is defined as

$$R_\alpha = \frac{100}{A_e} \left(\sum_h |\alpha_h - \langle \alpha_h \rangle| \right) \quad (3.33)$$

which this kind of fom proportionate with number of triplet that deviate from its expected statistical distribution. For right set of phases, this value have to be minimum. By computing different foms for each sets of phase deriving combined criterion correctness sets of phase (combined figure of merit, CFOM) is very useful. CFOM is more effective than other functions in separating sets of suitable phase. Minimum values of CFOM put forward that set of phase is true.

CHAPTER FOUR

CRYSTAL STRUCTURE REFINEMENT

4.1 Refinement Methods

When an approximate structure has been obtained using direct, Patterson or other methods, the atomic parameters that were determined with this method can be refined. Additional atoms can be located and their parameters also refined. These additional atoms are found using the Fourier synthesis method.

Two methods have been used for the refinement of the atomic positions and displacement (or temperature) parameters. One method is based on Fourier techniques, so called “Difference Fourier Method”, and the other is based on least-squares techniques, so called “Least-Squares Method”.

4.1.1 Difference Fourier Method

One way of the completing and refining a structural model is the “difference Fourier synthesis method”. In this method, we investigate the difference between experimental and calculated electron densities. We can write,

$$\rho_{cal}(\vec{r}) = \frac{1}{V} \sum_h \sum_k \sum_l F_{hkl}^{cal} \exp(-2\pi i \vec{h} \cdot \vec{r}) \quad (4.1)$$

for calculated electron density,

$$\rho_{obs}(\vec{r}) = \frac{1}{V} \sum_h \sum_k \sum_l F_{hkl}^{obs} \exp(-2\pi i \vec{h} \cdot \vec{r}) \quad (4.2)$$

for experimental electron density. In order to see how much the initial model deviates from the real structure, the difference series

$$\Delta\rho(\vec{r}) = \rho_{obs}(\vec{r}) - \rho_{cal}(\vec{r}) = \frac{1}{V} \sum_h \sum_k \sum_l [F_{hkl}^{obs} - F_{hkl}^{cal}] \exp(-2\pi i \vec{h} \cdot \vec{r}) \quad (4.3)$$

should be computed where F_{hkl}^{obs} and F_{hkl}^{cal} can be written as follows

$$F_{hkl}^{obs} = |F_{hkl}^{obs}| \exp(i\Phi^{obs}) \quad \text{and} \quad F_{hkl}^{cal} = |F_{hkl}^{cal}| \exp(i\Phi^{cal}) \quad (4.4)$$

Unfortunately the values of Φ^{obs} are not known and we have to assume $\Phi^{obs} \approx \Phi^{cal}$, will hold better the better is the initial model. (4.3) then becomes

$$\Delta\rho(\vec{r}) = \frac{1}{V} \sum_h \sum_k \sum_l [|F_{hkl}^{obs}| - |F_{hkl}^{cal}|] \exp(-2\pi i \vec{h} \cdot \vec{r} + i\Phi^{cal}) \quad (4.5)$$

If in the model an atom is missing, then $\rho_{cal}(\vec{r})$ will be zero at the corresponding position, while $\rho_{obs}(\vec{r})$ will show a maximum. The difference synthesis will also show a peak at the same position but it will be almost zero at the positions of model atoms where $\rho_{obs}(\vec{r}) \approx \rho_{cal}(\vec{r})$.

4.1.2 Least-Squares Method

By far the most widely used method of structure refinement is the “least-squares method” (Sparks, 1961; Cruickshank, 1970; Rollet, 1965). The crystallographic problem of determining the best set of atomic parameters that can be obtained from a set of experimental structure factors is usually solved with this method.

We can write the calculated structure factor, for a better set of atomic coordinates and temperature factors,

$$F_{hkl}^{cal} = \sum_{j=1}^{N/2} 2f_j \left(-B_j \frac{\sin^2 \theta}{\lambda^2} \right) \cos[2\pi(hx_j + ky_j + lz_j)] \quad (4.6)$$

where the structure is centrosymmetric and the temperature factor is isotropic. The correct values of parameters for j.th atom is as follows:

$$(B_j + \Delta B_j, x_j + \Delta x_j, y_j + \Delta y_j, z_j + \Delta z_j) \quad (4.7)$$

and the observed structure factor can be written as

$$F_{hkl}^{obs} = \sum_{j=1}^{N/2} 2f_j \exp \left[- (B_j + \Delta B_j) \frac{\sin^2 \theta}{\lambda^2} \right] \cos \left[2\pi \{ h(x_j + \Delta x_j) + k(y_j + \Delta y_j) + l(z_j + \Delta z_j) \} \right] \quad (4.8)$$

The difference of two expressions

$$\Delta F_{hkl} = F_{hkl}^{obs} - F_{hkl}^{cal} = \sum_{j=1}^{N/2} \left(\frac{\partial F_{hkl}^{cal}}{\partial B_j} \Delta B_j + \frac{\partial F_{hkl}^{cal}}{\partial x_j} \Delta x_j + \frac{\partial F_{hkl}^{cal}}{\partial y_j} \Delta y_j + \frac{\partial F_{hkl}^{cal}}{\partial z_j} \Delta z_j \right) \quad (4.9)$$

In order to gain the best approximation for observed structure factors, which are assumed to have no error in practice, the following expression must be minimum.

$$R_s = \sum_h [F_{hkl}^{obs} - F_{hkl}^{cal}]^2 \approx 0 \quad (4.10)$$

4.1.2.1 Overall Strategy

The overall strategy for crystallographic least-squares refinement depends on the size and nature of the problem, but some techniques can be mentioned here.

1. At the start of the refinement, the number of parameters should be minimized by refining only position and isotropic displacement parameters for the atoms that have been found from direct or Patterson methods (Section 4.1 and 4.2).
2. From a difference electron density map, other non-hydrogen atoms can be found and included in the refinement.
3. Anisotropic displacement parameters for the non-hydrogen atoms can be added. Hydrogen atoms cannot always be observed in difference electron density maps. However, hydrogen atoms can be placed at appropriate positions by using “riding” model constrains.
4. A final difference electron density map should always be calculated, to insure that no significant features of the structure have been left out of the refinement. Special attention should be given to possible disorder (large atomic displacement parameters for some atoms might be a clue), solvent molecules left out of the refinement or atoms (including hydrogen) that have been misplaced.

5. The estimated standard deviation and correlation coefficients for the refined parameters are calculated for the final refinement cycle.

4.2 Error Analysis

4.2.1 R Factors

Crystallographers often look first for the R-value as one of the simplest ways of evaluating the general results of a structural refinement. “R-value” shows the sensitivity between experimental and calculated data and can be written as

$$R = \frac{\sum_h \sum_k \sum_l |\Delta F_{hkl}|}{\sum_h \sum_k \sum_l |F_{hkl}^{obs}|} \quad \text{where} \quad \Delta F_{hkl} = |F_{hkl}^{obs}| - |F_{hkl}^{cal}|. \quad (4.11)$$

R-values ranges 0.4 – 0.5 at the starting of refinement and 0.02 – 0.06 at the end of the refinement.

Another R factor is R_w -value; called weighted R-value is given by

$$R_w = \frac{\sqrt{\sum_h \sum_k \sum_l w (\Delta F)^2}}{\sqrt{\sum_h \sum_k \sum_l w |F_{hkl}^{obs}|^2}} \quad (4.12)$$

where w is the weight function. (Guse, 2002)

4.2.2 Goodness of Fit

Another index obtained from the least-squares refinement is the “Goodness of Fit”,

$$GOF = \sqrt{\frac{\sum_h \sum_k \sum_l w \left[(F_{hkl}^{cal})^2 - (F_{hkl}^{obs})^2 \right]^2}{(n - m)}} \quad (4.13)$$

which is a measure of how well the distribution ΔF values fit the distribution expected for the weight which were used. Here n is the number reflections and m is the number of variables refined. GOF value must be nearly 1.0 in a perfect situation.

4.2.3 Final Difference Map

The final difference map provides a real-space counterpart for checking how well the refined model fits the experimental data, thus complimenting the R-factor which is a reciprocal-space measure. The final difference map should be featureless, with no peaks or holes of a magnitude greater than a few estimated standard deviations of the map values.

4.2.4 Estimated Standard Deviations

Also we search for sensitivity of atomic parameters at the end of determination. In order to determine the structure sensitively, the standard deviations must be less than 0.001 for coordinates, 0.01Å for bond distances and 1° for angles.

CHAPTER FIVE

COMPUTATIONAL METHODS

5.1 What is the Computational Chemistry?

Chemistry is an experimentally subject. In many areas of molecular physics, theoretical prediction of chemical properties can rival experimental measurement. The choice of whether to find the structure of a molecule, its bond lengths and and bond angles, by experimental spectroscopy or X-ray crystallography or by computation may come down to one of the convenience or cost.

Computational Chemistry is a new discipline and one of the fastest growing areas of chemistry. A sub-discipline of computational chemistry has grown up. This topic is distinct from theoretical chemistry. The activity involves taking known theory and developing the computer software to solve chemical problems. Its advent and popularity have paralleled improvements in computing power during the last several decades.

The challenges for computational chemistry are to characterize and predict the structure and stability of chemical systems, to estimate energy differences between different state, and to explain reaction pathways and mechanisms at the atomic level.

Methods prevalently used in computation process splits into two main classes: One of them is molecular mechanics and the other is quantum mechanical calculations. Furthermore, quantum mechanical calculations are also splitted into two parts called as *semi-empirical* methods and *ab initio* methods. Semi-empirical methods separate into many different sub-class within itself such as Extended

Hückel, CNDO, INDO, MINDO3, MNDO, MNDO/d, AM1, PM3, ZINDO/1, ZINDO/S and so on. In following sections, on these methods have been dealt with together its own outline.

5.2 Molecular Mechanics

Conformational analysis of a molecule is of importance to understand its stereochemical properties and molecular attitudes such as diversification of their polymerization process.

Just as the 1960s witnessed an explosion in the application of quantum mechanical methods that will be shown in the next chapter, there was a complementary interest in so-called "force field" methods for conformational analysis. The origin of these methods lies in vibrational spectra required the development of potential function to describe the overall molecular behaviour. Two different approaches were considered. In the first, the Central Force Field (CFF) method, the molecular vibration was fitted to a function that was a sum of pairwise interactions, without reference to the covalent structure of the molecule. The obvious disadvantage of this approach is that although such description is correct in terms of a quantum mechanical model of a molecule, it lacks the intuitive link with structure with which chemists are happier. The second method, the Valance Force Field (VFF), provides such a description in that the vibrational data is fitted to a potential function consisting of bond length and bond angle dependent terms. This is much more satisfactory and has the advantage of allowing comparisons between molecules; unlike the CFF potential functions which will be very molecule dependent. The major criticism of the VFF method is that the force constants produced must attempt to incorporate intramolecular interactions such as dispersion forces which result from electron correlation, and therefore are not simply a representation of the intrinsic vibrational frequency. These spectroscopic force fields provided the ideal starting point for what is now called molecular mechanics. By bringing together features from both the CFF and VFF methods, it proved possible to

derive energy functions that were at once chemically intuitive while still retaining the concept of through space attractions and repulsion.

The theoretical basis of the molecular mechanics method can be derived by taking an alternative approach to the Born-Oppenheimer approximation to that considered in molecular orbital methods: in this case the nuclear motion is considered while implying a fixed electron distribution associated each atom. To this end a model has been developed whereby a molecule is represented as a collection of spheres (possibly deformable) joined by springs. The motion of these atoms can then be described by the laws of classical physics and simple potential energy functions can be used. This allows much larger chemical system to be investigated. For instance, proteins and other biomolecules can only be investigated by molecular mechanics methods.

Although this method of calculation sounds ideal, the following caveats must be kept in mind. First, as the method neglects explicit representation of electrons, it is restricted principally to the discussion of molecular ground states. This also disallows the investigation of reactions. Secondly, the results obtained will only be as good as the potential functions and parameters used; much of potential energy surface defined by the force field has little validity as, typically, only extrema (stable conformations, rotational barriers etc.) are used in the parametrization procedure.

5.3. The Energy Calculation

The molecular representation introduced in the previous section was one that treated molecules as a set of vibrating spheres. The next step is to define an energy function which is consistent with this concept yet allows accurate calculations of molecular properties. The force field commonly encountered today have resulted from a number of generations of development. Typically, more structural and thermodynamic data have become available, coupled with considerable increases in computer power, allowing an extension of the functional form of energy calculation. As more terms are included, the accuracy of the force field increases.

The energy of a molecule is calculated as a sum of the steric and non-bonded interactions present. Therefore each bond length, angle and dihedral is treated individually while non-bonded interactions represent the influence of non-covalent forces.

$$E_{tot} = E_l + E_\theta + E_\omega + E_{nb} \quad (5.1)$$

Here E_l , E_θ , E_ω and E_{nb} are respectively the total bond, angle, dihedral and non-bonded energies. Explanations needed were done in following subsections.

5.3.1 Bond Stretch

The typical vibrational behaviour of a bond is near harmonic close to its equilibrium value but shows dissociation at longer bond lengths, as shown in Figure 5.1.

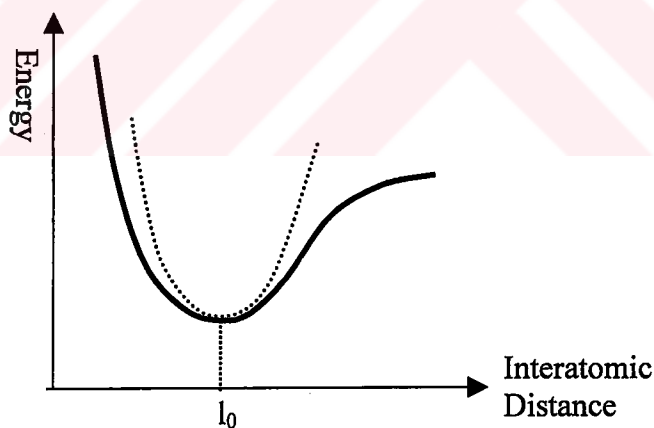


Figure 5.1 Morse Potential (Continuous line) and Harmonic Potential (Dashed line)

The most accurate description is the Morse potential function

$$E_l = \sum D_e \left[1 - e^{-\alpha(l-l_0)} \right]^2 \quad (5.2)$$

where l_0 is the equilibrium bond length, D_e the dissociation energy, and α a force constant. However, the exponential calculation is computationally expensive therefore most force fields have adopted a simple harmonic function

$$E_l = \sum k_l (l - l_0)^2 \quad (5.3)$$

k_l being the stretching force constant describing the deformation. The bond stretch is treated in the same fashion as a stretched spring. This equation has obvious limitation in that it only approximately describes the actual behaviour of the bond. Further, at extended bond length it is much too steep (see Figure 5.1), while it provides no representation of dissociation at very large deformation. When discussing minimization of poor geometries we will see that this can be an advantage as this function can allow more extended bonds to remain intact.

Other variations on equation (5.3) have been used to accommodate more accurate long distance behaviour. Most commonly this takes the form of an additional cubic term

$$E_l = \sum k_l (l - l_0)^2 + k_l' (l - l_0)^3 \quad (5.4)$$

but this suffers from the problem of inversion at long distance. Attempts have been made to remedy this by adding a quartic term which reverses the inversion.

5.3.2 Bond Angles

Historically, bond angles have been treated in the same way as bond lengths and are usually described by a harmonic function.

$$E_\theta = \sum k_\theta (\theta - \theta_0)^2 \quad (5.5)$$

As before, k_θ is a force constant and θ_0 the equilibrium value for the bond angle. Again, this term is not ideal for the full range of values observed so higher order terms must be added. In very strained ring systems, however, it is usually not possible to use the constants derived for unstrained and acyclic molecules so separate three- and four-membered ring constants have been developed.

5.3.3 Dihedral Angles

In very early force fields it was thought that this term could be omitted; gauche-trans energy differences would then result from non-bonded interactions. This soon proved to be an impossible task and dihedral angle terms were explicitly included. The functional form of this term is a Fourier series

$$E_{\omega} = \sum V_n (1 + s \cos n\omega) \quad (5.6)$$

where V_n is the rotational barrier height, n the periodicity of rotation (e.g. in ethane $n=3$; in ethene $n=2$) and $s=1$ for staggered minima and -1 for eclipsed minima. Figure 5.2 shows the $n=1, 2$ and 3 curves.

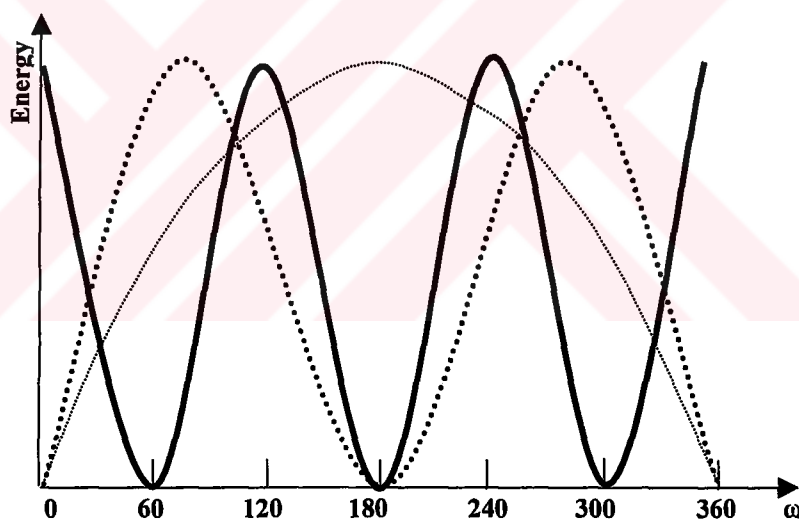


Figure 5.2 Variation of energy with dihedral angle for one (—), two (···) and threefold (---) barriers.

5.3.4 Non-bonded Interactions

The interactions discussed in the previous sections can also be grouped together as the bonded interactions, in the sense that they are defined by the connectivity of the molecule. The non-bonded interactions, on the other hand, are distance-dependent and are calculated as the sum over all atoms with a 1, 4 or greater separation. It is

usual to consider these interactions as having two components: van der Waals and electrostatic. The former can be considered as both a size parameter and representative of electron correlation (resulting from instantaneous dipole interactions), while the latter provides a quantitative measurement of the influence of polarity on the energy and structure.

Many different functional forms have been used for van der Waals interactions but the most common is the so-called 6-12, or Lennard-Jones potential

$$E_{vdw} = \sum \varepsilon \left[\left(\frac{r_m}{r} \right)^{12} - 2 \left(\frac{r_m}{r} \right)^6 \right] \quad (5.7)$$

ε is the well depth and r_m is the minimum energy interaction distance (see Figure 5.3). Short-range repulsions are accounted for by the r^{-12} term whereas London dispersion-attraction forces are mediated by the r^{-6} component. At short distance the repulsive term dominates. Other form have been proposed for the van der Waals interaction, so-called The Buckingham potential

$$E_{vdw} = Ae^{-Br} - Cr^{-6} \quad (5.8)$$

an exponential replaces the repulsive r^{-12} term. In most circumstances this function behaves similarly to the Lennard-Jones equation but at very short interatomic distances the function inverts and goes to $-\infty$, an obvious danger in poorly constructed model structures.

The second component of the non-bonded potential is the electrostatic term. This is usually calculated using partial charges (q) on the atom centers with the energy calculated using Coulomb's law

$$E_{el} = \sum \frac{q_i q_j}{Dr_{ij}} \quad (5.9)$$

with the dielectric constant D taking a value appropriate to a given solvent or made proportional to the distance r_{ij} between the charges. The electrostatic contribution is one of the most controversial in molecular mechanics.

5.3.5 Other terms

The five terms outlined above constitute the core of almost all molecular mechanics force fields; in some case the entire energy function. In many situations, however, it is necessary for additional terms to be included.

For systems where hydrogen bonding is vital for stability, e.g. biological molecules, it has been common to include an additional, explicit hydrogen bond energy function to ensure correct geometries. In certain protein force fields this takes the form

$$E_{hb} = \sum \left[\left(\frac{C_{ij}}{r_{ij}^{12}} \right) - \left(\frac{E_{ij}}{r_{ij}^{10}} \right) \right] \quad (5.10)$$

Other force field attempt to simulate hydrogen bonds using just the van der Waals and electrostatic terms without the inclusion of a special attractive potential.

Also, other commonly used terms, which are denominated cross terms, include stretch-bend, bend-bend, bend-torsion, are defined respectively in following: the stretch-bend term is

$$E_{l\theta} = \sum \sum k_{l\theta} (l - l_0)(\theta - \theta_0) \quad (5.11)$$

and the bend-bend term is

$$E_{\theta\theta'} = \sum \sum k_{\theta\theta'} (\theta - \theta_0)(\theta' - \theta_0)' \quad (5.12)$$

finally, torsion-bend term is

$$E_{\theta\theta'\omega} = \sum k_{\theta\theta'\omega} (\theta - \theta_0)(\theta' - \theta_0)' \cos \omega \quad (5.13)$$

where the k terms are the force constants; l , l_0 , θ , θ_0 and ω are as before.

5.4 Quantum Mechanical Calculations

Molecular mechanics calculations have been remarkably different from quantum mechanical calculations, because it has shortcomings such that covalent bonding of

atoms in a molecule does not explain. Quantum mechanical calculations (QMCs) are more preferable than molecular mechanical calculations that use principles of the Newtonian mechanics, since nature of covalent bonding can only be explained by quantum mechanical calculations. And also, choosing of calculating method to be used in determining of electronic structure of an molecule, as have been in many properties such as molecular orbitals, various geometric parameters, features of reactivity from frontier molecular orbital theory and so forth, is also of great importance in terms of time consuming or needed computer memory.

As mentioned before, QMCs are separated into two primary class called as *ab initio* and semi-empirical methods. In following, quantum mechanical calculating methods mentioned above were briefly disputed about their discriminative properties.

5.4.1 SCF Theory

The most clearly defined molecular orbital calculations are based on the Hartree-Fock (HF) or Self Consistent Field (SCF) method. For this reason, the method is of great importance in terms of computational molecular mechanics.

Hartree-Fock (HF) equation is defined as follows

$$H^{SCF} \phi_i = \varepsilon_i \phi_i \quad (5.14)$$

where

$$H^{SCF} = H^N + \sum_j J - \sum_j K \quad (5.15)$$

and the shorthand notation used is defined by

$$J_j \phi_i(1) = \left(\int |\phi_j(2)|^2 \frac{1}{r_{12}} dv_2 \right) \phi_i(1) \quad (5.16)$$

and

$$K_j \phi_i = \left(\int \phi_j(1) \phi_i(2) \frac{1}{r_{12}} dv_2 \right) \phi_i(1) \quad (5.17)$$

with a “–“ sign on a summation indicating summing only over pairs of electrons of the same spin.

The Hartree-Fock equations contain K_j or exchange terms in addition to the obvious Coulombic interelectron interactions allowed for in the Hartree equations. These exchange terms arise as a result of the Pauli principle that leads to determinantal wave function rather than products and exchange integrals between various cross products of the expanded determinant. The determinantal equation is defined as

$$\det|H^{SCF} - \epsilon S_{ik}| = 0 \quad (5.18)$$

where S_{ik} is known overlapping of the atomic orbitals that are take part in covalent bonding under discussion and defined as

$$S_{ik} = \int \chi_i \chi_k dv \quad (5.19)$$

where χ_m s are atomic orbitals. This equation solved after calculating all the integrals involved in H_{ik} and S_{ik} . Solution yields values of ϵ which are substituted in the secular equations to give new coefficients that determine to molecular wave function to be found. The process may then be repeated until the coefficients resulting from one cycle are identical within prescribed limits with those used in the previous cycle. The results are then self-consistent.

The various simplified methods of calculating molecular orbitals are essentially approximations of a greater or less drastic nature that result in a reduction of the number of the integrals necessary to build the matrix element H_{ik} and S_{ik} in the determinantal equation.

5.4.2 Configuration Interaction

We have already met the variation principle which tell us that the more flexible a wave function the better it will be in terms of the energy which results. One way of

improving the wave functions, which we have as a result of self-consistent field or approximate calculation is to allow the interaction of configuration.

Formally this means allowing a further linear mixing to give an improved wave function,

$$\Psi_{\text{improved}} = \sum_{i=0} c_i \Psi_i \quad (5.19).$$

In this expression ψ_0 is the wave function we first find and the others are wave functions that would be appropriate for excited configurations of the same symmetry. The coefficients above are mixing coefficient whose values are chosen so that energy improvement is maximized.

In many molecular orbital packages the effects of excited states are incorporated using perturbation theory as introduced by Moller and Plesset.

5.4.3 *Ab Initio* Method

All molecular wave functions are approximate; some are just more approximate than the others. We can solve the Schrödinger equation exactly for the hydrogen atom but not even, despite what many textbooks say, for the hydrogen molecule ion, H_2^+ . For the H_2^+ we make the Born-Oppenheimer approximation which separates electronic and nuclear motion, and calculate electronic energy of the ion with a given fixed internuclear distance and then obtain the total energy by adding the nuclear-nuclear repulsion term. In this method Hartree-Fock determinantal equation is solved by using Hartree-Fock self-consistent field operator. While doing it, each molecular orbital will be in the form

$$\phi_i = \sum_k c_{ik} \chi_{ik} \quad (5.20)$$

If the expansion is infinite then we would achieve the most flexible wave function within the constraints of the self-consistent field Hamiltonian which we have defined. The resulting energy would be the best we could obtain and is the Hartree-

Fock limiting energy. In practice, if an expansion of thirty or forty terms is used for ϕ , then little further improvement in energy results and we can safely assume that we are close to the limit. Most of difficulties encountered in calculations are related to matrix element of HF SCF Hamiltonian and calculate overlapping integrals. To overcome this problem we usually use different types of basis set, which are chosen to obey for our purposes. These functions chosen are separated into two main class within itself in terms of its radial parts. One that is denominated as Slater Type Orbital (STO) has radial weighting function in the form of $e^{-\zeta r}$ as zeta a parameter, and other that is denominated as Gaussian Type Orbital (GTO) has a more tractable form for the sake of facility of the calculations.

It is important to realize that even if we can afford to have long expansions of molecular orbitals and even reach the Hartree-Fock limit, there are still defects in the wave functions that arise from approximation in the actual Hartree-Fock equation.

There are two sources of error in the starting equations. The first comes about because the whole theory is based on the Schrödinger equation, which is not relativistically correct. Fast moving inner electrons may move with speeds which are not negligible by comparison with the velocity of light and relativistic effects thus contribute; mass is not constant. Since most chemical and biological transformations of molecules do not involve core electrons this error is normally a constant and causes no serious difficulty.

The second error is more than serious and is called the correlation energy error. This error or deviation from true values of energy stems from nature of Hartree-Fock method. In the method, progress accounting for interaction of one electron with another is not correct especially further stages in calculation, because in these stages correlation terms to be calculated were computed for interaction one electron with negative charge density consisted of more than one, whereas electron-electron correlation term can only be written in situation that both of electrons are also considered as point charge. In Figure 5.3, it has been shown Hartree-Fock limitation

and its utility in addition to influence of selection of basis set in *ab initio* method in comparison with true energy values.

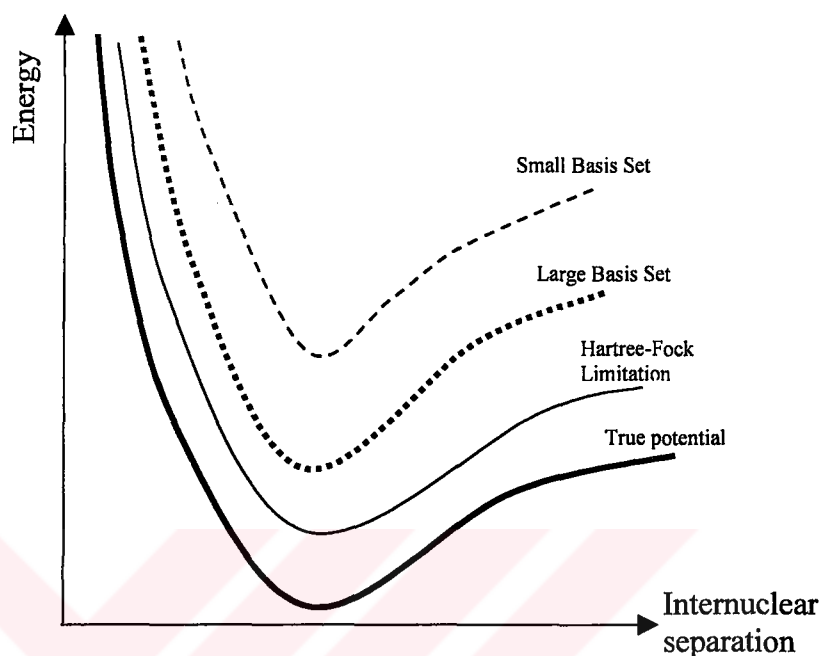


Figure 5.3 Energy values versus internuclear separation

5.4.4 Neglecting Differential Overlap (NDO)

Matrix element of Hartree-Fock self-consistent field Hamiltonian operator and overlapping integrals for a molecule composed of a large number of atoms are operations rigorous time consuming. While solving Hartree-Fock secular equation, for the sake of rapidly arriving to desired results, some approximations were proposed. Neglecting differential overlap is one of them.

In this approximation method, neglecting differential overlap of functions based on different centers, we eliminate not only all three or four center integrals but also most two or in occasion one-center integrals where different atomic orbitals are involved for either of two electrons.

NDO approximation has various types in terms of order and parameterization manner of neglecting in semi-empirical methods, as presented in the next subsection.

Some of them are denominated as CNDO, INDO, MINDO, MNDO, ZINDO/1, and ZINDO/S.

5.4.5 Semi-empirical Methods

Ab initio calculations are themselves not always perfectly successful in obtaining experimental observations. And also, the numbers of integrals to be calculated for even small molecules are numerous. In consequence, a great deal of effort has been expended devising so-called semi-empirical molecular orbital methods. These calculations start with determinantal equation but in following stage make various approximations to diminish the amount of consuming time.

All the commonly used techniques are valence electron calculations whereas 1s electrons can be neglected since these play little part in chemical or biochemical activities. The 1s electrons are defined as part of the core for first row atoms and both K and L shell electrons for heavier atoms. Thus, the self-consistent Hamiltonian becomes

$$H = H^{core} + \sum_j J_j - \sum_j K_j \quad (5.21)$$

and H^{core} contains kinetic energy and attraction to a core rather than to a bare nucleus. Integrals involving H^{core} are usually replaced by empirical or calculated parameters.

Semi-empirical methods cannot give more accurate results than *ab initio* methods due to the fact that it has parameters that are determined empirically. However, as long as the parametrization is related to experimental data that are closely with reference to parameters that are tried to be determined, then this approach works perfectly. Generally, semi-empirical methods using this idea give wide agreement with experimental results. Although results from semi-empirical methods can never be better than ones from *ab initio* method, they are more feasible than *ab initio* method, especially, in terms of time consumption.

The precision of the semiempirical methods is limited by the accuracy of the experimental data used in obtaining parameters. It should be noted, that it is frequently necessary to transform the experimental data before comparing to calculated results. It is also known that for precise comparison of *ab initio* total energies and semiempirical heat of formations with the experimental values, entropy corrections should be considered. This type of transformations were not performed consistently during the parametrization procedure of the above mentioned semiempirical methods. Parametrizing the semiempirical methods to reproduce the best available theoretical results would solve this problem. However, two serious problems remain: how to determine the best form of parametric functions and how to find the best minimum on the parameter hypersurface (Dewar & Ziegler, 1988). The development of the corrections to CRF illustrates the difficulties. It was found that the MNDO (Dewar & Thiel, 1977) parametrization is unable to describe correctly the core-core repulsion in crowded molecules.

Calculating methods chosen for performing the present master thesis are AM1 and PM3 methods. Next two subsections are dedicated to clarify details of AM1 and PM3 models with its comparison.

5.4.5.1 AM1 Method

Austin Model 1 that is progressed in the Texas University at Austin by Dewar and his collaborators have been improved through developing further either MNDO (Mixed Neglecting Differential Overlapping) or MINDO/3 (Mixed Intermediate Neglecting Differential Overlapping/3) approximations. While doing this improvement, new parameters that can be adjusted to fit experimental results are defined to arrive desired quantitative.

Extensive attempts to correct the errors in MNDO persuaded us that they had a common cause, a tendency to overestimate repulsions between atoms beyond van der Waals distance. The clear way to deal with this was to modify the core repulsion functions (CRF) in MNDO. But vain all the attempts to find a suitable functions in

order to enlighten on repulsions in question cannot be successful. Instead of this effort, innovators of his method would rather utilize by modifying available functions that represent the repulsions by additional Gaussian terms. The present form of AM1 probably represents about the best that can be achieved using the NDDO approximation as a basis, without specific allowance for the contributions of thermal energy. The CRF in it is as follows

$$CRF(AB) = z_A z_b \gamma_{ss} (1 + F(A) + F(B)) \quad (5.21)$$

where

$$F(A) = \exp(-\alpha_A R_{AB}) + \sum_i K_{A_i} \exp[L_{A_i} (R_{AB} - M_{A_i})^2] \quad (5.22)$$

$$F(B) = \exp(-\alpha_B R_{AB}) + \sum_j K_{B_j} \exp[L_{B_j} (R_{AB} - M_{B_j})^2] \quad (5.23)$$

The formalism used in AM1 method is essentially the same as that of used in MNDO with exception of the CRF. The values of L parameters, which define the widths of Gaussians, were not critical so a common value was used for most of them. They were not included in the overall optimization. The M and K parameters were all optimized. Note that the Gaussian terms, like the others in the CRF, refer to individual atoms, not pairs of atoms. In MNDO parameters were determined first for hydrocarbons and other elements were then added at a time. We had to do this because the number of molecules that could be included in the basis set for parameterization was limited by the computing time required. Development of a greatly improved optimization procedure has made possible the use of a much larger basis set, allowing parameters for C, H, O and N to be optimized in a single operation with a basis set which included some organic species. Parameters belonged to parameterization procedure used in AM1 are shown in Table 5.1.

Table 5.1 AM1 parameters for C, H, O and N atoms.

Parameters	E l e m e n t s			
	H	C	N	O
U_{ss}	-11.396427	-52.028658	-71.860000	-97.830000
U_{pp}		-39.614239	-57.167581	-78.262380
ζ_s	1.188078	1.808665	2.315410	3.108032
ζ_p		1.685116	2.157940	2.524039

β_s	-6.173787	-15.715783	-20.299110	-29.272773
β_p		-7.719283	-18.238666	-29.272773
α	2.882324	2.648274	2.947286	4.455371
K_1	0.122796	0.011355	0.025251	0.280962
K_2	0.005090	0.045924	0.028953	0.081430
K_3	-0.018336	-0.020361	-0.005806	
K_4		-0.001260		
L_1	5.000000	5.000000	5.000000	5.000000
L_2	5.000000	5.000000	5.000000	7.000000
L_3	2.000000	5.000000	2.000000	
L_4		5.000000		
M_1	1.200000	1.600000	1.500000	0.847918
M_2	1.800000	1.850000	2.100000	1.445071
M_3	2.100000	2.050000	2.400000	
M_4		2.650000		

The two strategies were used to modify the CRF and reduce excessive interatomic repulsion at large separations. In the first, one or more attractive Gaussians were added to compensate the excessive repulsions directly, centered in the region where the repulsions were excessive. In the second, repulsion Gaussians were centered at smaller internuclear separations, leading to an overall reduction of the main term in the expression for the core repulsion and hence reducing the repulsion at larger internuclear distances. In the case of carbon, hydrogen and nitrogen, both types of Gaussians were included, while only repulsive Gaussians were needed for oxygen. Attempts to use only repulsive Gaussians for the other elements led the poorer results while use of attractive Gaussian alone led to no improvement over MNDO.

5.4.5.2 PM3 Method

PM3 is a reparameterization of AM1, which is based on the neglect of diatomic differential overlap (NDDO) approximation. NDDO retains all one-center differential overlap terms when Coulomb and exchange integrals are computed. PM3

differs from AM1 only in the values of the parameters. The parameters for PM3 were derived by comparing a much larger number and wider variety of experimental versus computed molecular properties. Typically, non-bonded interactions are less repulsive in PM3 than in AM1. PM3 is primarily used for organic molecules, but is also parameterized for many main group elements.

The reparametrized AM1 method tried to remedy this problem by introducing Gaussian correction functions (GCF) to CRF. These corrections are outside the quantum-mechanical framework, their role is to adjust the nuclear-nuclear repulsion terms. Utilizing the GCF the AM1 method provided consistently superior results over the MNDO method. Later a fully optimized parameter set was produced by Stewart (Stewart, 1989). This parameter set is called PM3. The difference in parametrisation has been presented in Table 5.2, where a_{ik} , b_{ik} and c_{ik} are parameters that characterize Gaussian Correction Functions.

Table 5.2. GCF parameters for PM3 and AM1 methods.^a

Atom (<i>i</i>)	PM3 ^b				AM1 ^c		
	<i>k</i>	a_{ik}	b_{ik}	c_{ik}	a_{ik}	b_{ik}	c_{ik}
H	1	1.1288	5.10	1.5375	0.1228	5.00	1.20
	2	-1.0603	6.00	1.5702	0.0050	5.00	1.80
	3				-0.0183	2.00	2.10
C	1	0.0507	6.00	0.8925	0.0114	5.00	1.60
	2	0.0501	6.00	1.6422	0.0459	5.00	1.85
	3				-0.0200	5.00	2.05
	4				-0.0013	5.00	2.65
N	1	1.5017	5.90	1.7107	0.0253	5.00	1.50
	2	-1.5058	6.00	1.7161	0.0290	5.00	2.10
	3				-0.0058	2.00	2.40
O	1	-1.1379	5.95	1.5984	0.2810	5.00	0.848
	2	1.1311	6.00	1.6073	0.0814	7.00	1.445

^a Rounded values. ^b (Stewart, 1989). ^c (Dewar et al., 1985).

CHAPTER SIX

COMPUTATION TYPES

6.1 Introduction

In computational molecular mechanics, many different calculation methods have been appropriately improved to arrive our purposes, which are changing from one situation to another. Remarkable ones of them are single point, geometry optimization, transition state search, QSAR (Quantitative Structure Activity Relationships) analysis and so on (Grant & Richards, 1995).

In this chapter, two calculation methods utilized in my thesis of were elaborately discussed in the next sections.

6.2 Single Point Calculation

A single point calculation, as its name suggests, performs a calculation at only a single point on the potential surface, which specifies definite geometrical parameter set for given special molecular geometry. Normally, these calculations are for stationary points on a potential energy surface. Occasionally, you may want to characterize the potential energy surface by calculating the energies of a grid of points on the surface. You can use those results to generate a contour plot of the surface. You can use either molecular or quantum mechanical methods for single point calculations. The calculation provides energy and the gradient of that energy. The gradient is the root-mean-square of the derivative of the energy with respect to Cartesian coordinates. At a minimum the forces on atoms (the gradient) are zero. The size of the gradient can provide qualitative information to determine if a structure is

close to a minimum. Single point computation can use quantum mechanical methods to calculate several other properties. The properties include the dipole moment, total electron density, total spin density, electrostatic potential, heats of formation, orbital energy levels, vibrational normal modes and frequencies, infrared spectrum intensities, and ultraviolet-visible spectrum frequencies and intensities.

For a diatomic molecule, this might be a calculation at $R=2.0 \text{ \AA}$, for example. The results of a single point calculation give the potential energy of the system at that geometry, as well as the gradient at that point. For single parameter potential curves, the gradient describes the steepness of the potential curve at that point along the direction in which the energy decreases. For a polyatomic system, the situation is more complicated, but essentially the same the gradient gives the direction in which the energy goes most steeply downhill, along with the steepness of the down-hill slope. The RMS gradient that is reported is just the root-mean-square average of the Cartesian components of the gradient vector.

Most of using calculations needs to explore potential energy surface related to circumstance under study. A single point calculation determines the total energy and RMS (root mean square) gradient of a molecular system or of selected atoms. With a semi-empirical or *ab initio* method, single point also calculates the electron and charge distribution in the system. Single point the potential energy surface for the molecular system.

6.3 Geometry Optimization

Geometry optimizations find the coordinates of a molecular structure that represent a potential energy minimum. For a potential energy V and Cartesian coordinates r_i , the optimized coordinates satisfy this equation:

$$\frac{\partial V}{\partial r_i} = 0 \quad (6.1)$$

You might perform a geometry optimization calculation with one of these goals in mind:

- Characterize a potential energy minimum. A geometry optimization results in a new structure at a minimum. You can examine atomic coordinates and energy of this structure.
- Obtain a new stable structure as a starting point for a single point, quantum mechanical calculation, which provides a large set of structural and electronic properties.

There are three types of optimizers or algorithms: steepest descent, conjugate gradient such as Fletcher-Reeves and Polak-Ribiere, and block diagonal such as Newton-Raphson (Gill, 1981).

6.3.1 Steepest Descent

The steepest descent method is a first order minimizer. It uses the first derivative of the potential energy with respect to the Cartesian coordinates. The method moves down the steepest slope of the interatomic forces on the potential energy surface. The descent is accomplished by adding an increment to the coordinates in the direction of the negative gradient of the potential energy, or the force. The steepest descent method rapidly alleviates large forces on atoms. This is especially useful for eliminating the large non-bonded interactions often found in initial structures. Each step in a steepest descent requires minimal computing time. Its disadvantage is that convergence toward a minimum is very slow.

6.3.2 Conjugate Gradient

A conjugate gradient method differs from the steepest descent technique by using both the current gradient and the previous search direction to drive the minimization. A conjugate gradient method is a first order minimizer.

The advantage of a conjugate gradient minimizer is that it uses the minimization history to calculate the search direction, and converges faster than the steepest descent technique. It also contains a scaling factor, b , for determining step size. This makes the step sizes optimal when compared to the steepest descent technique.

6.3.3 Block Diagonal

The Newton-Raphson block diagonal method is a second order optimizer. It calculates both the first and second derivatives of potential energy with respect to Cartesian coordinates. These derivatives provide information about both the slope and curvature of the potential energy surface. Unlike a full Newton-Raphson method, the block diagonal algorithm calculates the second derivative matrix for one atom at a time, avoiding the second derivatives with respect to two atoms. This technique is available only for the MM+ force field. As is true for the conjugate gradient methods, you should *not* use this algorithm when the initial interatomic forces are very large (meaning, the molecular structure is far from a minimum).

6.3.4 Eigenvector Following

The Eigenvector Following method is in some ways similar to the Newton-Raphson method. Instead of explicitly calculating the second derivatives, it uses a diagonalized Hessian matrix to implicitly give the second derivatives of energy with respect to atomic displacements. The initial guess is computed empirically.

This method is available for all semi-empirical methods except Extended Hückel, and for *ab initio* calculations. This algorithm may be used if the structure is far from a minimum.

CHAPTER SEVEN

EXPERIMENTAL DETAILS

7.1 The Crystal of $C_{29}H_{25}N_3O_3$

7.1.1 Data Collection of $C_{29}H_{25}N_3O_3$ Crystal

Before starting data collection, the suitable crystals were selected from the synthesized crystals by using stereomicroscope and polarization microscope. Then a sample of size $0.08 \times 0.05 \times 0.26 \text{ mm}^3$ was selected for the crystallographic study.

The diffraction measurements were performed at room temperature ($293K$) on an Enraf-Nonius CAD-4 diffractometer using graphite-monochromated MoK_α radiation. Orientation matrix and unit cell parameters were obtained from the setting angles of 25 reflections at medium θ ($2.62^\circ < \theta < 23.11^\circ$). The systematic absences and intensity symmetries indicated the monoclinic $P2_1/n$ space group. A total of 3067 intensities with $\theta_{max}=23.11^\circ$ were collected in the $\omega/2\theta$ scan mode, as suggested by peak-shape analysis. The crystal and equipment stabilities were checked by the intensities of three standard reflections monitored every 120 minutes. No considerable amount intensity decay was observed throughout measurement under discussion. The intensities were corrected for Lorentz and Polarization factors, but not for absorption effect ($\mu = 0.086 \text{ mm}^{-1}$).

7.1.2 Structure Solution & Refinement of $C_{29}H_{25}N_3O_3$ Crystal

The structure was solved by direct methods using *SHELXS-97* for 1257 reflections satisfying $I > 4\sigma(I)$ and FOM values that used in phase determination are given in Table 6.1. Since the $\langle |E^2 - 1| \rangle = 0.898$, structure is centrosymmetric. The refinement (on F) was carried out by full-matrix least-squares method on the positional and anisotropic temperature parameters of the non-hydrogen atoms. Refinement of the structure was converged to $R=0.066$ for the observed reflections and $R=0.21$ for all data. The maximum peaks and minimum hole, observed in the final $\Delta\rho$ map, were 0.220 and $-0.230 e\text{\AA}^{-3}$, respectively. The scattering factors were taken from *SHELXL-97*. All of the H atoms were found in the difference-Fourier maps, and positions and isotropic thermal parameters were refined. The C-H bond distances range from 0.93(3) to 1.02(3) \AA , while U_{iso} values for H atoms are in the range 0.048(5)-0.120(1) \AA .

Table 7.1 FOM values for $C_{29}H_{25}N_3O_3$.

Set Code	R_α	NQUAL	MABS	CFOM
1049361	0.061	-0.658	1.068	0.124

7.1.3 Experimental Results for $C_{29}H_{25}N_3O_3$ Crystal

Table 7.2 Crystallographic data for $C_{29}H_{25}N_3O_3$.

Crystal Data	
Chemical formula	$C_{29}H_{25}N_3O_3$
Color/shape	White / prism
Formula weight (<i>a.m.u.</i>)	463.52
Space group	$P2_1/n$ (No.14)
Crystal system	Monoclinic / Centric

$\alpha, \beta, \gamma (^{\circ})$	90, 98.3860(10), 90
Cell volume (\AA^3)	2356.07(4)
Formula unit cell (Z)	4
D_x (g/cm^3)	1.3067(1)
F_{000}	976.0
Absorption coefficient μ (mm^{-1})	0.086
Crystal size (mm^3)	0.08x0.05x0.26

Data Collection	
Diffractometer	Enraf-Nonius CAD-4
Temperature (K)	293(2)
Scan type	$w/2\theta$
Radiation/Wavelength (\AA)	MoK $_{\alpha}$ / 0.71070
Reflections measured	3285
Independent/ Observed reflections	3067/1257
Range of h, k, l	0 \rightarrow 11, 0 \rightarrow 18, -14 \rightarrow 14
Standard reflections	3
Standards interval time (min)	120
Standards decay %	Less than 1%

Refinement	
Data/Restraints/Parameters	3067 / 0 / 317
Extinction Coefficient	0.0030(8)
Final R indices [$I > 4 \sigma(I)$]	0.0662
R indices (all data)	0.2104
$GooF$ (onF^2)	0.953
$\Delta\rho_{\min} / \Delta\rho_{\max}$ ($e/\text{\AA}^3$)	-0.23 / 0.22

$\Delta\rho_{\min} / \Delta\rho_{\max}$ ($e/\text{\AA}^3$)	-0.23 / 0.22
Weighting function	$w = 1/[\sigma^2(F_o^2) + (0.0579P)^2]$, where $P = (F_o^2 + 2F_c^2)/3$

Table 7.3 Atomic coordinates and equivalent isotropic thermal parameters (\AA^2).

<i>Atom</i>	<i>x</i>	<i>y</i>	<i>z</i>	U_{eq}^a
O1	-0.1874(4)	0.2274(3)	-0.1730(3)	0.065(2)
O2	-0.0962(3)	0.2367(2)	-0.0105(3)	0.056(2)
O3	0.5531(4)	-0.0875(3)	0.1661(3)	0.067(2)
N1	0.2016(4)	0.1566(3)	0.0694(3)	0.039(2)
N2	0.0303(4)	0.2355(3)	0.0437(3)	0.045(2)
N3	0.0288(4)	0.2432(3)	-0.1287(3)	0.043(2)
C1	0.0672(5)	0.1471(3)	0.0599(4)	0.041(2)
C2	0.2265(5)	0.2121(3)	-0.0114(4)	0.052(2)
C3	0.1082(5)	0.2643(3)	-0.0337(4)	0.038(2)
C4	-0.0936(6)	0.2341(4)	-0.1122(5)	0.050(3)
C5	0.5149(6)	-0.1675(4)	0.1872(5)	0.083(3)
C6	0.4596(6)	-0.0328(4)	0.1418(4)	0.047(3)
C7	0.4973(5)	0.0445(4)	0.1232(5)	0.059(3)
C8	0.4125(6)	0.1068(4)	0.0986(4)	0.054(3)
C9	0.2849(5)	0.0915(3)	0.0917(4)	0.040(2)
C10	0.2483(5)	0.0142(4)	0.1108(4)	0.048(2)
C11	0.3344(5)	-0.0480(3)	0.1361(4)	0.049(3)
C12	0.0182(5)	0.1154(3)	0.1516(4)	0.037(2)
C13	0.0671(6)	0.1410(4)	0.2473(5)	0.057(3)
C14	0.0207(7)	0.1134(4)	0.3292(5)	0.069(3)
C15	-0.0771(7)	0.0615(4)	0.3188(5)	0.064(3)
C16	-0.1307(6)	0.0331(4)	0.2257(6)	0.063(3)
C17	-0.0816(5)	0.0613(3)	0.1412(5)	0.054(3)

C19	0.1964(6)	0.3821(4)	0.0695(5)	0.058(3)
C20	0.2230(7)	0.4631(5)	0.0859(6)	0.073(3)
C21	0.1826(7)	0.5190(4)	0.0114(7)	0.070(3)
C22	0.1149(6)	0.4942(4)	-0.0777(6)	0.064(3)
C23	0.0885(5)	0.4121(4)	-0.0940(5)	0.053(3)
C24	0.0700(5)	0.2313(4)	-0.2235(4)	0.0389(1)
C25	0.1704(5)	0.2733(4)	-0.2490(4)	0.050(2)
C26	0.2074(5)	0.2628(4)	-0.3411(4)	0.051(2)
C27	0.1473(6)	0.2092(4)	-0.4091(5)	0.059(3)
C28	0.0518(6)	0.1637(4)	-0.3828(5)	0.067(3)
C29	0.0099(6)	0.1749(4)	-0.2914(5)	0.058(3)

^a U_{eq} is defined as one third of the trace of the orthogonalized U_{ij} tensor.

Table 7.4 Anisotropic displacement parameters of non-hydrogen atoms.

<i>Atom</i>	U_{11}	U_{22}	U_{33}	U_{23}	U_{13}	U_{12}
O1	0.038(3)	0.093(3)	0.063(3)	0.022(3)	0.001(2)	-0.002(2)
O2	0.038(3)	0.078(3)	0.057(3)	0.022(3)	0.022(2)	0.011(2)
O3	0.056(3)	0.053(3)	0.091(4)	0.019(3)	0.003(3)	0.015(2)
N1	0.032(3)	0.044(3)	0.044(3)	0.013(2)	0.007(2)	0.001(2)
N2	0.034(3)	0.052(3)	0.053(3)	0.017(3)	0.019(2)	0.012(2)
N3	0.030(3)	0.055(3)	0.048(3)	0.005(3)	0.010(2)	-0.002(2)
C1	0.035(3)	0.049(4)	0.039(4)	0.006(3)	0.001(3)	-0.002(3)
C2	0.036(3)	0.056(4)	0.065(5)	0.014(4)	0.014(3)	0.010(3)
C3	0.030(3)	0.048(4)	0.041(4)	0.013(3)	0.017(3)	0.004(3)
C4	0.047(4)	0.050(4)	0.053(5)	0.018(4)	0.004(4)	0.013(3)
C5	0.065(5)	0.056(5)	0.129(7)	0.025(5)	0.016(4)	0.017(4)
C6	0.051(4)	0.038(4)	0.053(5)	0.004(3)	0.006(3)	0.011(3)
C7	0.031(4)	0.062(5)	0.081(5)	0.009(4)	0.000(3)	0.003(4)
C8	0.051(4)	0.044(4)	0.066(5)	0.005(3)	0.006(3)	-0.005(3)
C9	0.043(4)	0.030(4)	0.045(4)	0.001(3)	0.004(3)	0.000(3)
C10	0.044(4)	0.049(4)	0.050(4)	0.007(3)	0.005(3)	-0.001(3)

C11	0.043(4)	0.041(4)	0.064(5)	0.012(3)	0.007(3)	-0.002(3)
C12	0.043(4)	0.038(3)	0.032(4)	0.010(3)	0.012(3)	0.005(3)
C13	0.072(5)	0.064(5)	0.038(4)	-0.001(4)	0.015(4)	-0.010(4)
C14	0.063(5)	0.095(6)	0.050(5)	0.000(4)	0.010(4)	-0.004(4)
C15	0.064(5)	0.079(5)	0.056(5)	0.017(4)	0.028(4)	0.006(4)
C16	0.050(4)	0.066(5)	0.074(5)	0.015(4)	0.010(4)	-0.008(3)
C17	0.052(4)	0.048(4)	0.058(5)	0.005(4)	-0.005(3)	-0.002(3)
C18	0.034(3)	0.046(4)	0.050(4)	-0.002(4)	0.013(3)	-0.002(3)
C19	0.069(5)	0.053(4)	0.053(5)	0.003(4)	0.008(4)	-0.006(4)
C20	0.077(5)	0.078(6)	0.063(5)	0.002(5)	0.008(4)	-0.003(4)
C21	0.072(5)	0.048(5)	0.094(7)	-0.011(5)	0.029(5)	-0.014(4)
C22	0.075(5)	0.055(5)	0.070(6)	0.015(4)	0.035(4)	0.014(4)
C23	0.056(4)	0.046(4)	0.058(5)	0.011(4)	0.016(3)	0.014(3)
C24	0.033(3)	0.054(4)	0.029(3)	0.004(3)	0.002(3)	0.005(3)
C25	0.043(4)	0.058(4)	0.050(4)	-0.006(4)	0.015(3)	-0.004(3)
C26	0.047(4)	0.062(4)	0.049(4)	-0.002(4)	0.021(3)	-0.007(3)
C27	0.075(5)	0.064(5)	0.042(4)	-0.005(4)	0.023(4)	-0.006(4)
C28	0.078(5)	0.058(5)	0.068(5)	-0.007(4)	0.019(4)	-0.011(4)
C29	0.059(4)	0.066(5)	0.049(4)	-0.002(4)	0.011(4)	-0.020(4)

Table 7.5 Bond distances (Å) in the title molecule.

Atoms	Bond distance	Atoms	Bond distance
O1 -C4	1.209(8)	O2 -N2	1.452(6)
C18-C23	1.364(9)	O2 -C4	1.366(8)
C19-C20	1.375(11)	O3 -C5	1.421(8)
C18-C19	1.400(9)	C20-C21	1.380(11)
O3-C6	1.357(8)	C21-C22	1.367(12)
N1-C1	1.449(7)	C22-C23	1.392(9)
N1-C2	1.470(7)	C24-C25	1.371(8)
N1-C9	1.404(7)	C24-C29	1.392(9)

N2-C1	1.516(7)	C25-C26	1.361(8)
N2-C3	1.504(7)	C26-C27	1.362(9)
N3-C3	1.468(7)	C27-C28	1.363(9)
N3-C4	1.381(8)	C28-C29	1.377(9)
N3-C24	1.418(7)	C1-H1	0.9790
C1-C12	1.499(7)	C2-H2A	0.9702
C2-C3	1.534(7)	C2-H2B	0.9698
C3-C18	1.525(7)	C5-H5A	0.9602
C6-C7	1.370(9)	C5-H5B	0.9608
C6-C11	1.368(9)	C5-H5C	0.9587
C7-C8	1.383(9)	C7-H7	0.9303
C8-C9	1.392(9)	C8-H8	0.9300
C9-C10	1.368(8)	C10-H10	0.9294
C10-C11	1.392(8)	C11-H11	0.9298
C12-C13	1.378(8)	C13-H13	0.9295
C12-C17	1.390(7)	C14-H14	0.9299
C13-C14	1.349(10)	C15-H15	0.9308
C14-C15	1.351(10)	C16-H16	0.9289
C15-C16	1.377(10)	C17-H17	0.9302
C16-C17	1.397(10)	C19-H19	0.9304
C20-H20	0.9298	C26-H26	0.9301
C21-H21	0.9292	C27-H27	0.9291
C22-H22	0.9296	C28-H28	0.9300
C23-H23	0.9298	C29-H29	0.9304
C25-H25	0.9299		

Table 7.6 Bond Angles ($^{\circ}$) in the molecule.

<i>Atoms</i>	<i>Bond Angle</i>	<i>Atoms</i>	<i>Bond Angle</i>
N2 -O2 -C4	110.0(4)	C7 -C8 -C9	119.8(6)
C5 -O3 -C6	115.8(5)	N1 -C9 -C8	118.3(5)

C1	-N1	-C2	107.0(4)	N1	-C9	-C10	123.8(5)
C1	-N1	-C9	122.7(4)	C8	-C9	-C10	117.8(5)
C2	-N1	-C9	116.8(4)	C9	-C10	-C11	121.9(5)
O2	-N2	-C1	107.1(4)	C6	-C11	-C10	120.0(5)
O2	-N2	-C3	103.5(4)	C1	-C12	-C13	121.4(5)
C1	-N2	-C3	103.8(4)	C1	-C12	-C17	120.2(5)
C3	-N3	-C4	109.9(4)	C13	-C12	-C17	118.4(5)
C3	-N3	-C24	125.9(4)	C12	-C13	-C14	120.9(6)
C4	-N3	-C24	124.1(5)	C13	-C14	-C15	120.5(6)
N1	-C1	-N2	98.5(4)	C14	-C15	-C16	121.9(6)
N1	-C1	-C12	115.8(4)	C15	-C16	-C17	117.4(6)
N2	-C1	-C12	109.5(4)	C12	-C17	-C16	120.9(6)
N1	-C2	-C3	104.7(4)	N1	-C2	-C3	104.7(4)
N2	-C3	-N3	101.9(4)	C3	-C18	-C23	124.9(6)
N2	-C3	-C2	103.0(4)	C19	-C18	-C23	118.5(5)
N2	-C3	-C18	109.3(4)	C18	-C19	-C20	120.8(6)
N3	-C3	-C2	113.7(4)	C19	-C20	-C21	119.7(7)
N3	-C3	-C18	112.4(4)	C20	-C21	-C22	120.2(7)
C2	-C3	-C18	115.1(4)	C21	-C22	-C23	119.9(7)
O1	-C4	-O2	122.4(6)	C18	-C23	-C22	120.9(6)
O1	-C4	-N3	129.2(6)	N3	-C24	-C25	121.1(5)
O2	-C4	-N3	108.4(5)	N3	-C24	-C29	119.9(5)
O3	-C6	-C7	115.4(6)	C25	-C24	-C29	119.0(5)
O3	-C6	-C11	126.0(6)	C24	-C25	-C26	120.6(5)
C7	-C6	-C11	118.6(6)	C25	-C26	-C27	120.8(6)
C6	-C7	-C8	121.8(6)	C26	-C27	-C28	119.3(6)
C27	-C28	-C29	121.0(6)	C15	-C14	-H14	119.79
C24	-C29	-C28	119.1(6)	C14	-C15	-H15	119.06
N1	-C1	-H1	110.78	C16	-C15	-H15	119.08
N2	-C1	-H1	110.82	C15	-C16	-H16	121.34
C12	-C1	-H1	110.75	C17	-C16	-H16	121.28
N1	-C2	-H2A	110.80	C12	-C17	-H17	119.53

N1	-C2	-H2A	110.80	C12	-C17	-H17	119.53
N1	-C2	-H2B	110.80	C16	-C17	-H17	119.61
C3	-C2	-H2A	110.77	C18	-C19	-H19	119.52
C3	-C2	-H2B	110.84	C20	-C19	-H19	119.70
H2A	-C2	-H2B	108.86	C19	-C20	-H20	120.15
O3	-C5	-H5A	109.47	C21	-C20	-H20	120.20
O3	-C5	-H5B	109.48	C20	-C21	-H21	119.93
O3	-C5	-H5C	109.55	C22	-C21	-H21	119.84
H5A	-C5	-H5B	109.39	C21	-C22	-H22	120.04
H5A	-C5	-H5C	109.43	C23	-C22	-H22	120.09
H5B	-C5	-H5C	109.49	C18	-C23	-H23	119.50
C6	-C7	-H7	119.12	C22	-C23	-H23	119.59
C8	-C7	-H7	119.04	C24	-C25	-H25	119.71
C7	-C8	-H8	120.05	C26	-C25	-H25	119.69
C9	-C8	-H8	120.10	C25	-C26	-H26	119.59
C9	-C10	-H10	119.03	C27	-C26	-H26	119.59
C11	-C10	-H10	119.07	C26	-C27	-H27	120.36
C6	-C11	-H11	119.98	C28	-C27	-H27	120.35
C10	-C11	-H11	120.00	C27	-C28	-H28	119.48
C12	-C13	-H13	119.51	C29	-C28	-H28	119.49
C14	-C13	-H13	119.55	C24	-C29	-H29	120.53
C13	-C14	-H14	119.70	C28	-C29	-H29	120.38

Table 7.7 Torsion angles ($^{\circ}$) in the molecule.

<i>Atoms</i>				<i>Torsion Angles</i>	<i>Atoms</i>				<i>Torsion Angles</i>
N2	-O2	-C4	-O1	173.5(6)	N2	-O2	-C4	-N3	-8.7(6)
C4	-O2	-N2	-C3	21.3(5)	C4	-O2	-N2	-C1	-88.0(5)
C5	-O3	-C6	-C11	0.0(8)	C5	-O3	-C6	-C7	179.0(5)
C2	-N1	-C1	-C12	-161.3(4)	C9	-N1	-C1	-N2	176.3(4)
C2	-N1	-C1	-N2	-44.7(5)	C2	-N1	-C9	-C8	44.2(7)

C1	-N1	-C2	-C3	26.5(5)	C1	-N1	-C9	-C10	-2.9(8)
C4	-N3	-C3	-C18	-96.2(6)	C3	-N3	-C4	-O1	169.4(7)
C3	-N3	-C4	-O2	-8.4(6)	C24	-N3	-C3	-C18	85.5(7)
C24	-N3	-C4	-O2	170.0(5)	C3	-N3	-C24	-C25	-31.5(9)
C3	-N3	-C24	-C29	147.0(6)	C4	-N3	-C24	-C25	150.4(6)
C4	-N3	-C24	-C29	-31.0(9)	C4	-N3	-C3	-N2	20.8(6)
C24	-N3	-C4	-O1	-12.3(11)	C4	-N3	-C3	-C2	130.8(5)
N1	-C1	-C12	-C13	40.4(7)	N2	-C1	-C12	-C17	107.8(5)
N1	-C1	-C12	-C17	-142.0(5)	N2	-C1	-C12	-C13	-69.8(7)
N1	-C2	-C3	-N2	3.6(5)	N1	-C2	-C3	-N3	-105.8(5)
N1	-C2	-C3	-C18	122.5(5)	N2	-C3	-C18	-C19	63.1(6)
C2	-C3	-C18	-C23	127.4(6)	N2	-C3	-C18	-C23	-117.3(6)
N3	-C3	-C18	-C19	175.5(5)	N3	-C3	-C18	-C23	-4.9(8)
C2	-C3	-C18	-C19	-52.2(7)	C11	-C6	-C7	-C8	-0.3(9)
O3	-C6	-C11	-C10	179.6(5)	O3	-C6	-C7	-C8	-179.3(5)
C9	-N1	-C2	-C3	168.3(4)	C1	-N1	-C9	-C8	179.6(5)
O2	-N2	-C1	-N1	155.3(4)	O2	-N2	-C3	-N3	-24.4(5)
O2	-N2	-C3	-C2	-142.4(4)	O2	-N2	-C3	-C18	94.8(5)
C1	-N2	-C3	-N3	87.3(4)	O2	-N2	-C1	-C12	-83.4(5)
C3	-N2	-C1	-N1	46.2(4)	C3	-N2	-C1	-C12	167.6(4)
C1	-N2	-C3	-C18	-153.5(4)	C1	-N2	-C3	-C2	-30.7(5)
C24	-N3	-C3	-N2	-157.5(5)	C24	-N3	-C3	-C2	-47.5(7)
C7	-C6	-C11	-C10	0.7(8)	C6	-C7	-C8	-C9	-0.3(9)
C7	-C8	-C9	-C10	0.6(8)	C7	-C8	-C9	-N1	178.2(5)
N1	-C9	-C10	-C11	-177.7(5)	C8	-C9	-C10	-C11	-0.2(8)
C9	-C10	-C11	-C6	-0.4(8)	C13	-C12	-C17	-C16	-0.4(8)
C1	-C12	-C17	-C16	-178.1(5)	C1	-C12	-C13	-C14	178.6(6)
C17	-C12	-C13	-C14	1.0(9)	C12	-C13	-C14	-C15	-1.7(10)
C13	-C14	-C15	-C16	1.8(11)	C14	-C15	-C16	-C17	-1.2(10)
C15	-C16	-C17	-C12	0.5(9)	C3	-C18	-C19	-C20	78.2(6)
C19	-C18	-C23	-C22	1.2(9)	C23	-C18	-C19	-C20	-1.4(9)
C3	-C18	-C23	-C22	-78.4(6)	C18	-C19	-C20	-C21	0.3(11)

C19	-C20	-C21	-C22	1.0(12)	C20	-C21	-C22	-C23	-1.1(11)
C21	-C22	-C23	-C18	0.0(10)	C25	-C24	-C29	-C28	-0.9(9)
N3	-C24	-C25	-C26	-78.5(6)	C29	-C24	-C25	-C26	2.9(9)
N3	-C24	-C29	-C28	-79.5(6)	C24	-C25	-C26	-C27	-0.4(10)
C25	-C26	-C27	-C2	-0.3(10)	C26	-C27	-C28	-C29	4.3(10)
C27	-C28	-C29	-C24	-0.7(10)					

Table 7.8 Weak interactions to be regarded as weak hydrogen bonds (Å).

<i>D—H...A</i>	<i>D—H</i>	<i>H...A</i>	<i>D...A</i>	<i>D—H...A</i> (°)
C(11) -- H(11)···O(1)	0.9298	2.5091	3.424(7)	167.90
C(13) -- H(13)···O(1)	0.9295	2.5651	3.471(8)	165.05
C(23) -- H(23)···N(3) ⁱ	0.9298	2.5386	2.877(8)	101.83
C(29) -- H(29)···O(1) ⁱⁱ	0.9304	2.4978	2.965(8)	111.30

Symmetry operation:

- (i) $-x, -y, -z$
(ii) $1/2+x, 1/2-y, 1/2+z$

Table 7.9 Standard deviations of atoms from the some remarkable planes (°).

Plane 1		Plane 2		Plane 3		Plane 4	
<i>Atoms</i>	<i>Deviations</i> (Å)	<i>Atoms</i>	<i>Deviations</i> (Å)	<i>Atoms</i>	<i>Deviations</i> (Å)	<i>Atoms</i>	<i>Deviations</i> (Å)
* [†] C1	-0.291(5)	*C3	0.140(5)	*C1	-0.493(5)	*C1	0.006(5)
*C2	-0.059(5)	*C4	0.001(7)	*C2	0.036(5)	*C5	0.020(7)
*C3	-0.109(5)	*N2	-0.142(5)	*C3	0.588(5)	*C6	-0.010(5)
*N1	0.218(4)	*N3	-0.093(5)	*C4	-0.436(7)	*C7	-0.003(7)
*N2	0.241(4)	*O2	0.094(3)	*N1	-0.241(5)	*C8	-0.001(5)
O(2)	-0.612(4)	O(1)	0.042(5)	*N2	0.648(5)	*C9	-0.015(5)

O(3)	-0.112(4)	C(2)	-0.921(5)	*N3	-0.363(5)	*C10	-0.017(5)
N(3)	-1.468(4)	C(24)	-0.408(7)	*O2	0.261(3)	*C11	-0.010(5)
C(15)	1.264(8)	C(29)	-1.240(7)	O(1)	-0.966(5)	*N1	0.025(4)
C(18)	0.874(6)	C(27)	-0.999(7)	C(7)	-1.371(7)	*O3	0.004(4)

† Asterisks indicate atoms passing through the planes.

Table 7.10 Dihedral angles between the planes ($^{\circ}$).

<i>Planes</i>	<i>Dihedral Angle</i>	<i>Planes</i>	<i>Dihedral Angle</i>
1-2	60.0(3)	1-3	28.3(3)
2-3	31.7(3)	3-4	47.6(2)
2-4	75.6(3)	1-4	27.6(3)

7.1.4 Molecular Graphics of $C_{29}H_{25}N_3O_3$ Crystal

An ORTEP3 diagram of the molecular structure of the title compound is shown in Figure 7.1, with the atom-numbering scheme. Figure 7.2 shows the packing of the title compound in the unit cell and the network of weak interactions to be regarded as weak hydrogen bonding formed among C, N and O atoms. A space-filling (CPK) model with van der Waals radii assigned to each atom is given in Figure 7.3.

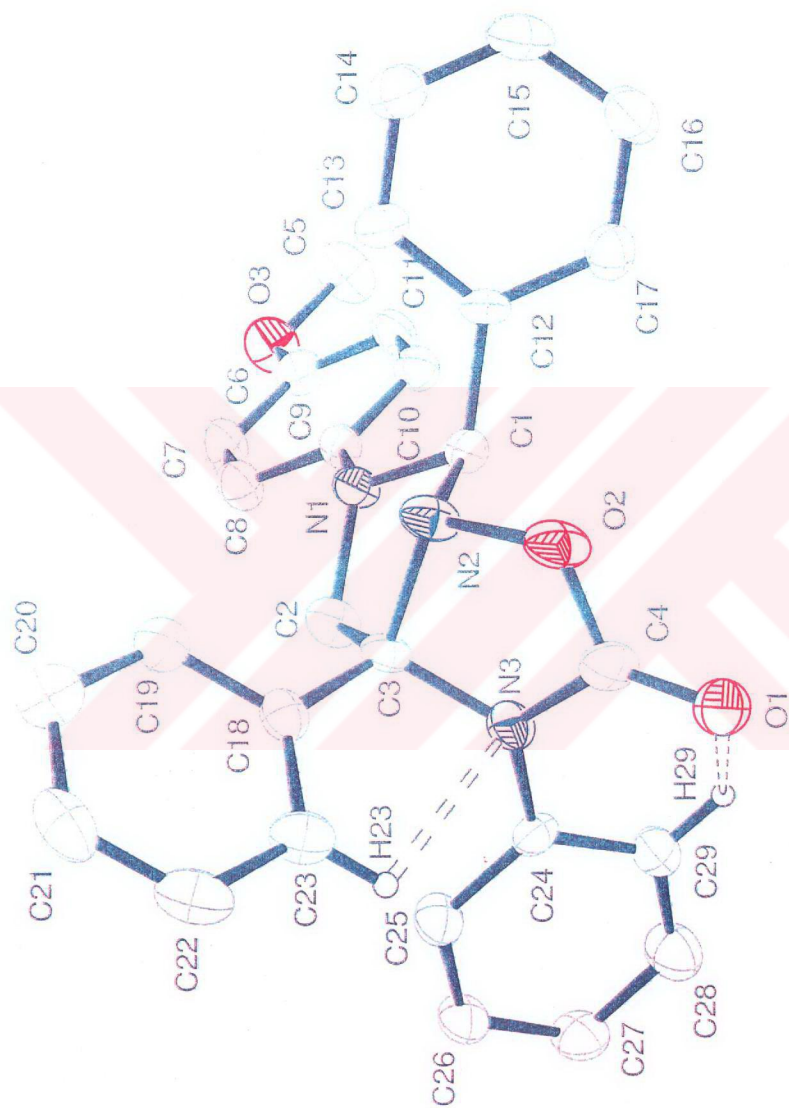


Figure 7.1 An ORTEP3 drawing of $C_{29}H_{25}N_3O_3$ showing the intramolecular weak interactions. Displacement ellipsoids of non-H atoms are shown at the 30% probability level.

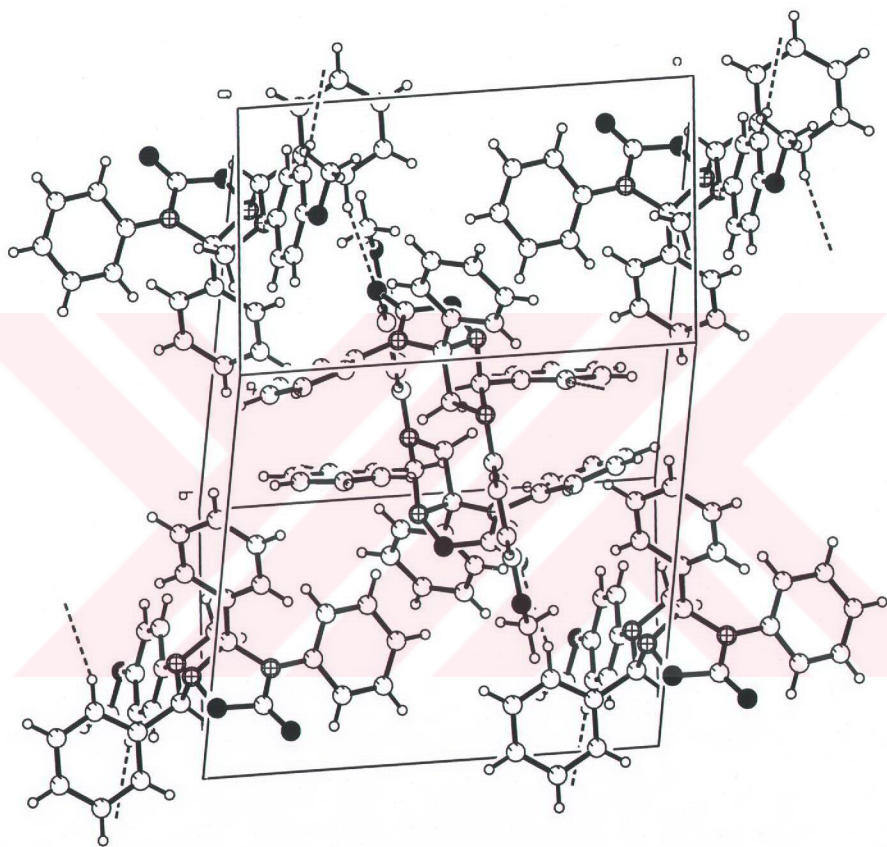


Figure 7.2 Unit cell contents with the weak interactions scheme indicated by dashed lines via PLUTO program.

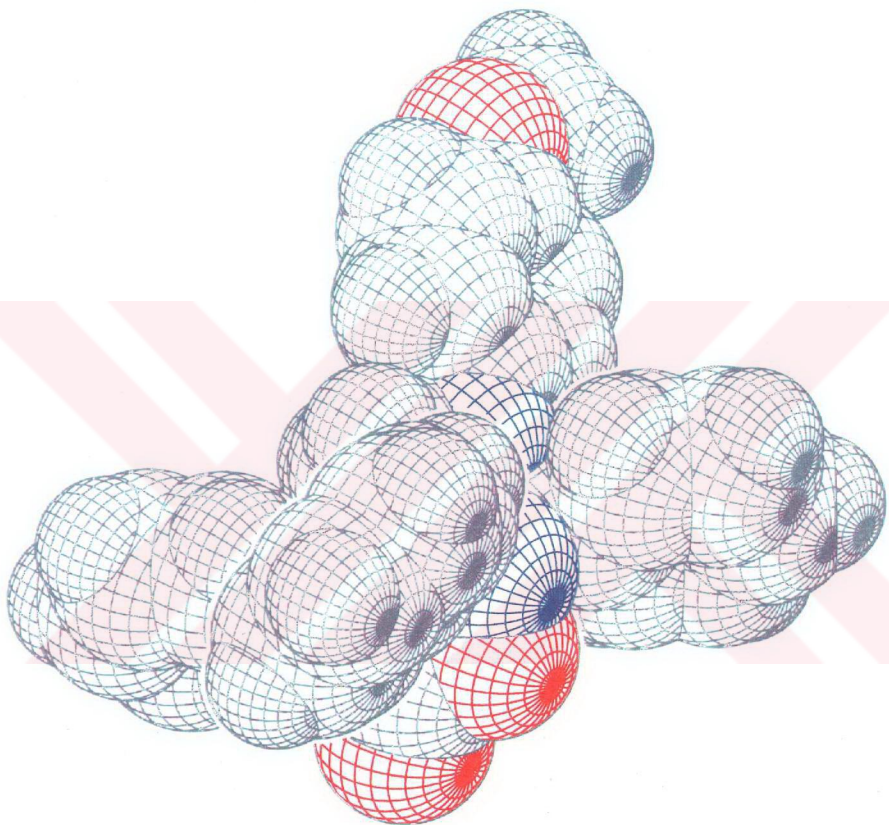


Figure 7.3 A CPK drawing C₂₉H₂₅N₃O₃.

7.2 Computational Details for the Molecule

Geometry optimization of the title molecule was achieved by means of AM1 and PM3 self-consistent fields molecular orbital SCF MO semi-empirical method at the spin-restricted Hartree-Fock (RHF) level (Roothaan, 1951) via application of a conjugate gradient method, which is called as Polak-Ribiere algorithm (Fletcher, 1990), with RMS gradient 0.1 kcal/Å mol. To obtain conformational energy profiles versus selected dihedral angles, geometry of the title compound from X-ray crystallographic data was entirely optimized without any symmetry constraints. For a selected dihedral angle, while keeping other dihedral angles constant, it was initially set to zero and varied in every 10°. Heats of formation values corresponding to each conformer were calculated as function of the four dihedral angles T1(C8-C9-N1-C2), T2(C13-C12-C1-N1), T3(C25-C24-N3-C3) and T4(C19-C18-C3-C2) from -180° to +180° via single point calculations on computed potential energy surface belonged to the molecule. All the calculations were performed by using HyperChem 6.0 package programme for Windows on Intel Pentium II computer.

Results from single point calculations belonged to optimized free molecular geometry of the molecule were given in Table 7.11 and Table 7.12 and these results were exhibited in Figure 7.4- Figure 7.7.

Table 7.11 Conformational energy values versus torsion angles from -180° to +180° by AM1 semi-empirical method.

Torsion Angle (°)	Heat of Formations (kcal/mol)			
	E ₁ = E ₁ (T1)	E ₂ = E ₂ (T2)	E ₃ = E ₃ (T3)	E ₄ = E ₄ (T4)
-180.00	106.94	105.76	108.80	109.81
-170.00	105.84	105.50	116.87	108.62
-160.00	104.80	105.03	125.85	107.02
-150.00	104.68	104.94	131.59	107.43
-140.00	105.66	106.60	129.28	111.79
-130.00	107.12	110.76	121.13	119.06

-120.00	107.99	115.32	113.36	126.02
-110.00	107.74	117.25	109.08	127.68
-100.00	106.79	116.18	109.59	122.74
-90.00	105.95	115.28	112.85	114.52
-80.00	105.53	116.72	115.84	107.53
-70.00	105.35	118.24	116.00	104.04
-60.00	105.23	116.86	112.80	103.07
-50.00	105.15	112.87	108.31	103.24
-40.00	105.29	108.80	104.99	104.25
-30.00	105.85	106.11	103.37	106.82
-20.00	106.66	104.67	103.07	111.22
-10.00	106.98	103.92	104.24	115.55
00.00	106.20	103.49	108.32	117.37
10.00	104.66	103.22	116.49	115.64
20.00	103.37	103.04	126.02	112.05
30.00	103.07	103.18	132.77	110.52
40.00	103.87	104.26	131.38	115.08
50.00	105.35	106.75	123.00	125.52
60.00	106.57	109.47	114.73	139.37
70.00	106.83	111.08	109.89	143.90
80.00	106.26	112.77	110.02	135.52
90.00	105.57	116.92	112.97	123.75
100.00	105.22	123.35	115.54	113.09
110.00	105.15	127.44	115.29	107.13
120.00	105.16	125.29	111.96	105.12
130.00	105.19	118.71	107.74	104.88
140.00	105.33	111.69	104.79	105.13
150.00	105.80	107.46	103.44	105.95
160.00	106.60	105.92	103.30	107.60
170.00	107.21	105.75	104.59	109.34
180.00	106.94	105.76	108.80	109.81

Table 7.12 Conformational energy values versus torsion angles from -180° to $+180^\circ$ by PM3 semi-empirical method.

Heat of Formations (kcal/mol)				
Torsion Angle ($^\circ$)	$E_1 = E_1(T1)$	$E_2 = E_2(T2)$	$E_3 = E_3(T3)$	$E_4 = E_4(T4)$
-180.00	47.19	50.66	66.69	48.65
-170.00	47.03	49.99	75.76	48.10
-160.00	47.37	49.34	88.84	47.33
-150.00	47.62	48.33	87.99	47.62
-140.00	47.37	47.17	70.94	48.35
-130.00	47.23	47.59	60.27	48.54
-120.00	47.37	48.20	51.68	53.96
-110.00	47.35	48.12	48.57	59.35
-100.00	47.37	49.75	47.61	62.80
-90.00	47.74	55.24	46.80	61.10
-80.00	47.82	60.43	46.59	57.05
-70.00	47.58	63.81	46.48	51.88
-60.00	47.46	63.92	46.54	49.13
-50.00	47.53	60.09	46.95	47.03
-40.00	47.43	54.95	47.67	46.88
-30.00	46.95	52.82	49.42	47.72
-20.00	46.82	51.05	52.95	47.87
-10.00	46.81	50.12	58.54	49.60
0.00	46.42	49.57	70.55	50.99
10.00	46.18	48.96	85.63	50.53
20.00	46.37	48.40	113.55	48.60
30.00	46.49	47.80	118.41	47.35
40.00	46.45	46.74	84.98	48.05
50.00	46.39	46.51	65.85	48.30
60.00	46.62	47.04	55.27	53.69
70.00	46.83	47.56	49.82	60.36
80.00	46.98	50.49	48.69	66.67

90.00	47.44	57.09	47.54	66.39
100.00	47.73	63.25	47.19	60.62
110.00	47.59	67.94	47.16	54.89
120.00	47.51	67.80	47.48	48.67
130.00	47.60	64.15	48.17	47.46
140.00	47.69	57.50	48.80	47.98
150.00	47.34	54.35	49.96	48.08
160.00	47.17	52.39	52.65	47.73
170.00	47.31	51.22	57.19	48.24
180.00	47.19	50.66	66.69	48.65

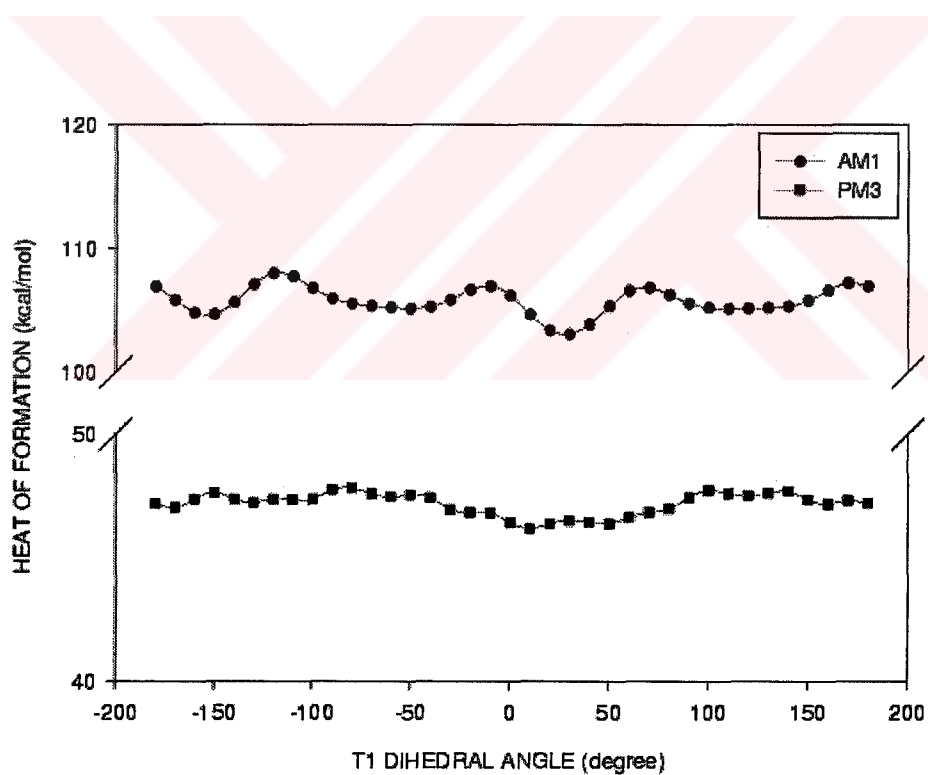


Figure 7.4 Calculated energy profiles of the molecule by AM1 and PM3 semi-empirical method with respect to T1.

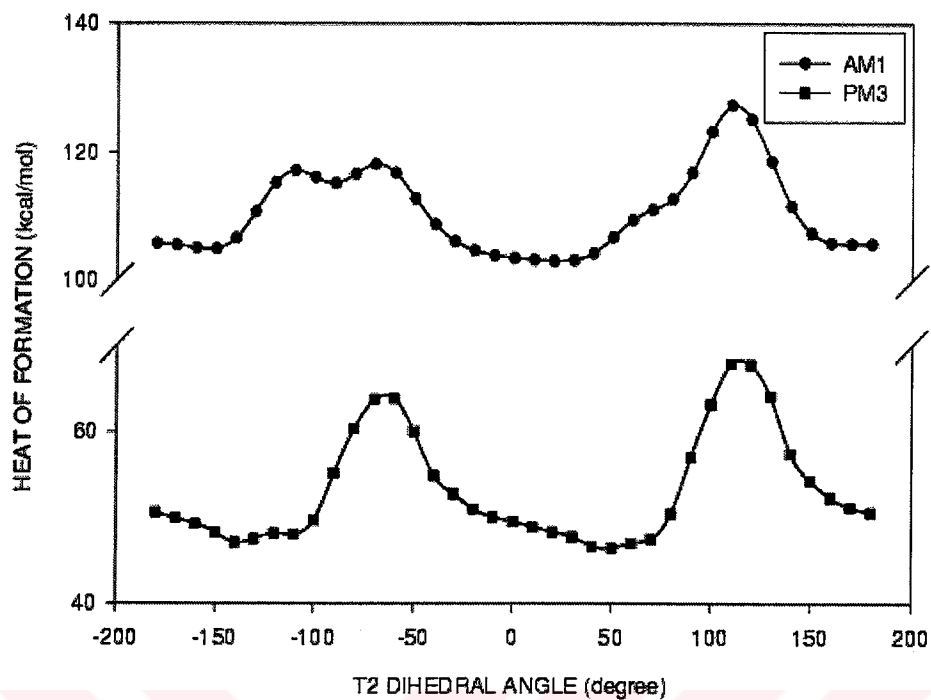


Figure 7.5 Calculated energy profiles of the molecule by AM1 and PM3 semi-empirical method with respect to T2.

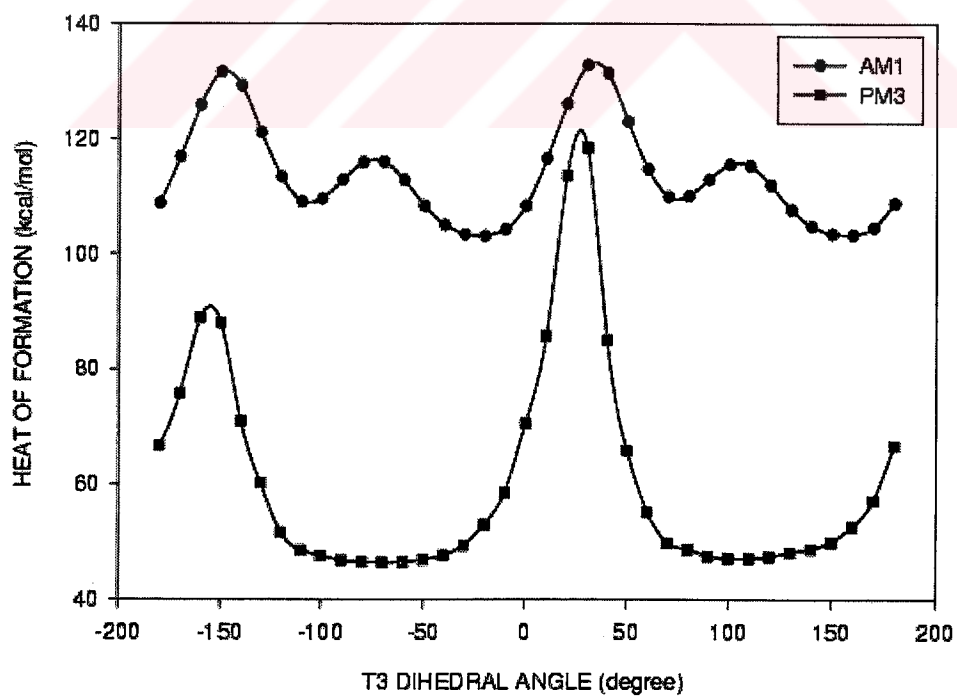


Figure 7.6 Calculated energy profiles of the molecule by AM1 and PM3 semi-empirical method with respect to T3.

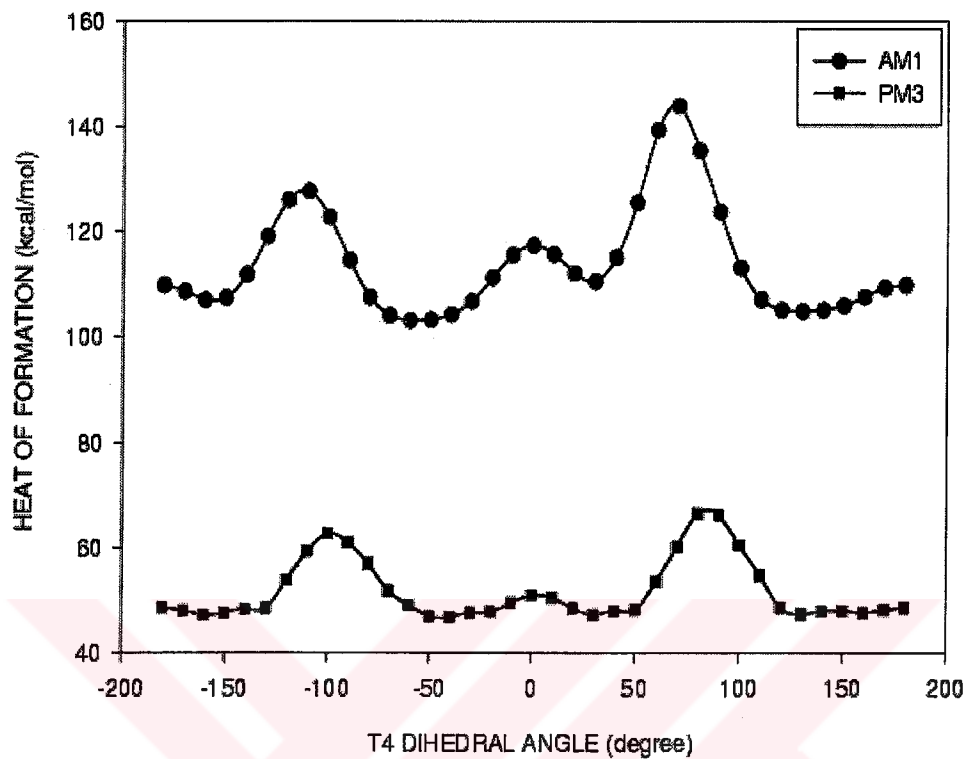


Figure 7.7 Calculated energy profiles of the molecule by AM1 and PM3 semi-empirical method with respect to T4.

CHAPTER EIGHT

CONCLUSIONS

8.1 Conclusions Related to X-Ray Crystallographic Study

In this study, molecular and crystal structures of 6-(4-methoxy-phenyl)-1,5,7a-triphenyl-tetrahydro-imidazo[1,5-*b*][1,2,4]oxadiazol-2-one, $C_{29}H_{25}N_3O_3$ has been determined by single crystal X-ray diffraction technique and then following results have been concluded.

Results from X-ray crystallography, which are given in Table 7.5, Table 7.6 and Table 7.7 are in consistence with ones reported for part of resembling compounds in the literature (Zhaoa et al., 2000; Pulitia et al., 2000; Glowiaaka & Kurdzielb, 2000; Castineiras et al., 2000; Jina et al., 2001). Values of T1, T2, T3 and T4 dihedral angles from X-ray investigations are $44.2(7)^\circ$, $40.4(7)^\circ$, $-31.5(9)^\circ$ and $-52.2(7)^\circ$, respectively. When experimental data given in Table 8.1 are contrasted with data from theoretical calculations related to optimized geometry of the title molecule, both of them are seen to be generally in consistence. All phenyl and substituted phenyl rings in the molecule, as expected, are nearly planar. Oxygen atom of the methoxy group is located at the same plane where 4-methoxyphenyl lies in. The angle between planes that are respectively defined by C18-23 and C24-29 atoms is $62.6(3)^\circ$. The fact that these phenyl rings have different orientation relative to other phenyl rings can be explained by dominating both of weak interactions. One of the five membered rings through O2, N2, C3, N3, and C4 atoms is in twisted conformation and the other through N1, C1, N2, C3, and C2 atoms are in envelope conformation (Cremer et al., 1975). C1 atom has maximum deviating [$-0.291(5)$ Å] from average ring plane of five membered rings, which consists of N1, C1, N2, C3,

and C2 atoms adopting envelope conformation. C18...C23 and C12...C17 phenyl rings are attached to the five membered ring under discussion as bisectonal (neither equatorial nor axial) and equatorial respectively, in addition, 4-methoxyphenyl ring is equatorially linked to this ring, and finally, phenyl ring C24...C29 is also equatorially attached to the twisted five membered ring. Five membered ring having twisted conformation is fused with a ring having envelope conformation by bonding (N2-axial (Evans et al., 1989), C3-bisectonal). There are two asymmetric carbon atoms (C1 and C3) are in the molecule. C1 and C3 carbon atoms have R and S chiral configurations, respectively.

8.2. Conclusions Related to Computational Aspects

In order to define conformational flexibility of the title molecule, semi-empirical calculations using AM1 and PM3 self-consistent field molecular orbital theories parameterized by empirical data were performed. The molecular energy is thought as separated into two parts. One of these parts is bonded energy term, which is independent of changing in dihedral angles, and the other is non-bonded, which depends on changing in dihedral angles such as dihedral, steric and electrostatic contributions. Steric effects have been of great significance for the determination of molecular energy profile as mentioned in the following interpretations.

Values of T1, T2, T3 and T4 dihedral angles in structure optimized by AM1 are 27.53°, 24.56°, -22.33° and -57.17°, respectively and by PM3 are 26.87°, 46.90°, -65.32° and -44.87°, respectively. Molecular structure from X-ray crystallography is of no enormous difference from those calculated by AM1 and PM3 methods. Another significant differentiation to be taken into consideration between X-ray structure and calculated molecular models is also that the five membered rings at core of the molecule are adapted to different conformations from those obtained by X-ray crystallographic study. These five membered rings prefer to be in nearly planar conformations according to calculation results. While calculating, any semi-empirical method as well as AM1 and PM3 cannot consider both intra- and intermolecular interactions. For that reason, it is not astonishing that five membered

rings of the molecule prefer to be in nearly planar conformation as different from results obtained by X-ray crystallographic study. Although five membered rings of the X-ray structure are non-planar, the most stable conformation is planar in terms of five membered rings. A reason for arising situation under discussion is the fact that the molecule is regarded as isolated (or free) molecule during calculations. According to calculated heat of formation values with respect to selected dihedral angles, the most stable conformer of the title molecule is of general consistence with structure obtained from X-ray crystallography except for conformations of the five membered rings. Also, many local maximums to be construed are observed in Figure 7.4. And also, optimized geometrical parameters belonged to the molecule, which were given in Table 8.1 have been exhibited to compare with the values from crystallographic studies. Since PM3 was parametrized better than AM1, it gives us more appropriate results in terms of X-ray results.

Table 8.1 Selected bond distances (Å) and bond angles (°) with ESDs in parentheses and their values calculated by AM1 and PM3 semi-empirical method.

		X-ray	AM1	PM3
O1	-C4	1.209(8)	1.226	1.212
O2	-N2	1.452(6)	1.356	1.513
O2	-C4	1.366(8)	1.412	1.361
O3	-C5	1.421(8)	1.422	1.406
O3	-C6	1.357(8)	1.382	1.382
N1	-C1	1.449(7)	1.480	1.507
N1	-C2	1.470(7)	1.454	1.494
N1	-C9	1.404(7)	1.415	1.447
N2	-C1	1.516(7)	1.480	1.499
N2	-C3	1.504(7)	1.549	1.513
N3	-C3	1.468(7)	1.483	1.512
N3	-C24	1.418(7)	1.408	1.451
C2	-C3	1.534(7)	1.578	1.547
N3	-C4	1.381(8)	1.404	1.440

C5	-O3	-C6	115.8(5)	115.9	117.36
C1	-N1	-C2	107.0(4)	109.6	109.31
O2	-N2	-C1	107.1(4)	108.8	109.67
O1	-C4	-O2	122.4(6)	116.4	116.92
O2	-N2	-C3	103.5(4)	106.2	107.92
N2	-C3	-N3	101.9(4)	104.3	103.28
C3	-N3	-C4	109.9(4)	108.1	108.67
N2	-O2	-C4	110.0(4)	112.5	107.77
C1	-N2	-C3	103.8(4)	105.6	110.14
N1	-C1	-N2	98.5(4)	110.1	105.89
N2	-C3	-C2	103.0(4)	106.0	105.63
O2	-C4	-N3	108.4(5)	109.0	112.29
N3	-C3	-C18	112.4(4)	114.4	111.70
N1	-C2	-C3	104.7(4)	107.9	106.96

Because the most deviation from energy minimum in the energy profile as a function of T1 are less than 5 kcal/mol by AM1 and 1.6 kcal/mol by PM3, these variations related to T1 dihedral angle do not cause any remarkable effects on conformational flexibility of the molecule. From this profile, four maximums are seen in Figure 7.4 according to AM1. These local maximums and fluctuations from PM3 seen in the figure are due to orientation of 4-meyhoxyphenyl ring relative to the remaining parts of the molecule not to any steric hindrance among hydrogen atoms. It is deduced from this profile that dihedral energy term, which is a non-bonded interaction, should be considered as minor contribution to molecular energy.

The energy profile obtained as a function of T2 dihedral angle in both AM1 and PM3 methods has a drastic maximum in vicinity close to 110° in Figure 7.5. The peak arises from steric hindrance between hydrogen atoms aromatically linked to C17 and C10, respectively. Another evident peak in this profile is one appeared in vicinity close to -75°. This peak arises from steric hindrance between hydrogen atoms aromatically linked to C10 and C13 atoms.

For T3 dihedral angle, two evident peaks are observed in Figure 7.6 according to AM1. The peak appeared in vicinity close to 30° is stemmed from steric hindrance between hydrogen atoms aromatically and axially linked to C25 and C2, respectively and the other appeared near -150° is stemming from breaking intra-molecular weak interaction C29-H29...O1. In PM3 calculations for T3, solely two maximums are observed. One that appears nearby 30° is sharper than the other appeared nearby -155° . While breaking this intra-molecular weak interaction distance between hydrogen and acceptor increases from 2.4978 Å to 4.627 Å and energy needed to break this interaction is estimated 42.52 kcal/mol according to PM3. For this reason, according to PM3, steric hindrance between hydrogen atoms is remarkable than the intra-molecular weak interaction in terms of molecular flexibility.

The obtained energy profile as a function of T4 dihedral angle has a drastic maximum in vicinity close to 80° in both AM1 and PM3 methods. This peak is due to the steric hindrance between hydrogen atoms aromatically linked to C19 and C25, respectively. According to PM3, as T4 in vicinity close to 0° , C23-H23...N3 weak interaction is brought and the distance between hydrogen and the acceptor is increased from 2.546 Å to 2.895 Å. It is inferred from Figure 7.7 that this breaking energy is roughly 4.11 kcal/mol. When these two interactions are compared with the each other in terms of their own strength, the fact that estimated breaking energy value for interaction C29-H29...O1 is more than interaction C23-H23...N3 have been also confirmed by X-ray investigation presented Table 7.8. Other remarkable peak in Figure 7.7 is near -90° . This peak appears because of steric hindrance between hydrogen atoms aromatically linked to C23 and C25, respectively.

In summary, the AM1 and PM3 optimized geometry of the molecule is of generally consistence with ones crystallographically observed except for five membered rings at the core of the molecule. In all crystallographic molecular and crystal structures of the title molecule were elucidated and it was seen that results obtained from each of these studies are generally in agreement and both of weak interactions in addition to steric hindrance arising between ortho-hydrogens to be

regarded as each of non-bonded contributions to molecular energy play an important role in determination of the conformational flexibility of the molecule. As mentioned before, when donations arising from both intra-and intermolecular contacts are taken into account of, steric hindrances between ortho-hydrogen atoms dominate to those expressed above and supply leading contribution to non-bonded energy term for the molecule.



REFERENCES

- Aygün, M. (1997). Tek Kristal X-Işınları Kırınımı Yöntemiyle C₁₂H₁₀N₄O₄S, C₁₆H₁₈ClO₂PS ve C₁₇H₁₅ClO₃ Moleküllerinin Kristal Yapı Çözümü. Samsun: Doktora Tezi.
- Castineiras, A., Gomez, M. C., Sevillano, P. (2000). 2-(2,3-Dihydro-1,3-benzothiazol-2-yl)phenyl(diphenyl) phosphine oxide. Synthesis and characterization by IR and NMR spectroscopy and X-ray diffractometry. Journal of Molecular Structure, 554, 301-306.
- Cochran, W. (1952). A relation between the signs of structures factors. Acta Cryst., 5, 65-67.
- Cochran, W. (1953). Sayre's equation and Zachariasen's method. Acta Cryst., 6, 810-811.
- Cochran, W. (1954). The determination of signs of structure factors from the intensities. Acta Cryst., 7, 581-583.
- Cochran, W. & Woolfson, M. M. (1955). The theory of sign relations between structure factors. Acta Cryst., 8, 1-12.
- Cochran, W. (1955). Relations between the phase of structure factors. Acta Cryst., 8, 473-478.
- Corsaro, A., Pistarà, V., Rescifina, A., Romeo, G., Romeo, R., Chiacchio, U. (2002).

- 1,3-Dipolar cycloadditions of acridine with nitrile oxides. ARKIVOC, (viii), 5-15.
- Coşkun, N. & Sümengen, D. (1993). Synthesis Communication, 24, 165-167.
- Coşkun, N. (1997). Regio and Diastereoselective Addition of Imidazole 3-oxides to Aryl Isocyanates. Tetrahedron, 53, 13873-13882.
- Coşkun, N. (1997). Tetrahedron Lett., 38, 2299.
- Cremer, D. & Pople, J. A. (1975). Journal of American Chemical Society, 97, 1354.
- Cruickshank, D. W. J. (1970). Crystallographic Computing. Copenhagen: Munksgaard.
- Dewar, M. J. S., Zoebisch, E. G., Healy, E. F., Stewart, J. J. P. (1985). AM1: A New General Purpose Quantum Mechanical Molecular Model. Journal of the American Chemical Society, 107, 3902-3909.
- Dewar, M. J. S. & Zoebisch, E. G. (1988). J. Molecular Structure, 180, 1.
- Dewar, M. J. S. & Thiel, W. (1977). J. American Chemical Society, 99, 4899.
- Dunitz, J. D. (1979). X-Ray Analysis and Structure of Organic Molecules. U.S.A.: Cornell University Press.
- Enraf-Nonius Inc. (1993). Diffractometer Control Software Release 5.1. The Netherlands
- Evans, G. G. & Boeyens, J. A. (1989). Acta Cryst. B45, 581.
- Farrugia, L. J. (1997). Ortep3 for Windows. Journal of Applied Crystallography, 30, 565.

- Farrugia, L. J. (1999). WinGX. Journal of Applied Crystallography, 32, 837-838.
- Fischer, R., Drucková, A., Fiserá, L., Hametner, C. (2002). Preparation and 1,3-dipolar cycloadditions of chiral nitrones derived from D-xylose with vinyl acetate. ARKIVOC, (viii), 80-90.
- Fletcher P. (1990). Practicle Methods of Optimization. New York: J. Wiley.
- Giacovazzo, C., Monaco H. L., Artioli, G., Viterbo, D., Ferraris, G., Gilli, G. (1998). Fundamentals of Crystallography. Oxford: Oxford University Press.
- Gill, P.E., Murray, W., Wright, M.H. (1981). Practical Optimization. New York: Academic Press.
- Gillis, J. (1948). Structure factor relations and phase determination. Acta Cryst., 1, 76-80.
- Głowiaka, T. & Kurdzielb, K. (2000). Crystal structure and physico-chemical properties of heptacoordinate isomorphous cobalt(II) and nickel(II) complexes of 1-allylimidazole. Journal of Molecular Structure, 516, 1-5.
- Goedkoop, J. A. (1950). Remarks on the theory of phase limiting inequalities and equalities. Acta Cryst., 3, 374-378.
- Gökçe, A. G. (2002). The Crystal Structure Analysis of C₂₈H₂₄N₂O₂ and C₂₃H₃₂N₄Se by Single Crystal X-ray Diffraction Technique. İzmir: Yüksek Lisans Tezi.
- Grant, H. G. & Richards, W. G. (1995). Computational Chemistry. Oxford: Oxford University Press.

- Harker, D. & Kasper, J. S. (1948). Phases of Fourier coefficient directly from crystal diffraction data. Acta Cryst., **1**, 70-75.
- Hauptman, H. & Karle, J. (1956). A theory of phase determination for the four types non-centrosymmetric space groups 1P222, 2P22, 3P₁2, 3P₂2. Acta Cryst., **9**, 635-651.
- HyperCube Software Inc. (1996). HyperChem Computational Chemistry Package Program. Canada.
- Jina, Z., Xua, D., Pana, Y., Xua, Y., Chiangb, M. Yen-Nan. (2001). 2:1 Complex of 4-methylphenol with piperazine, structure in the solid and solution state. Journal of Molecular Structure, **559**, 1-5.
- Karle, J. & Hauptman, H. (1950). The phases and magnitudes of the structure factors. Acta Cryst., **3**, 258-261.
- Karle, J. & Hauptman, H. (1956). A theory of phase determination for the Four types of non-centrosymmetric space groups 1P222, 2P22, 3P₁2, 3P₂2. Acta Cryst., **9**, 635-651.
- Karle, J. & Hauptman*, H. (1956). Structure invariants and seminvariants for non-centrosymmetric Space Groups. Acta Cryst., **9**, 45-55.
- Karle, J. & Hauptman, H. (1961). Seminvariants for non-centrosymmetric space groups with conventional centered cells. Acta Cryst., **14**, 217-223.
- Kopfmann, G. & Huber, R. (1968). A Method of Absorption Correction by X-ray Intensity Measurement. Acta Cryst. **A24**, 348-351.
- Ladd, M. F. C. & Palmer, R. A. (1988). Structure Determination by X-ray Crystallography. (2nd ed.). New York, London: Plenum Press.

- Lecture Notes for the Tenth Summer School "Course In Crystallography". (2001). Structure Analysis by X-ray Crystallography. (4th ed.). American Crystallographic Association: University of Georgia, USA.
- Luger, P. (1980). Modern X-Ray Analysis on Single Crystal. Berlin: Walter de Gruyter.
- MacGillavry, C. H. (1950). On the derivation of Harker-Kasper inequalities. Acta Cyst., 3, 214-217.
- Motherwell, W. D. S. & Cleegg, W. (1978). PLUTO. Program for Plotting Molecular and Crystal Structures. University of Cambridge, England.
- Norman, R.O.C. (1978). Principles of Organic Synthesis. London: Chapman and Hall.
- Pulitua, R., Mattiab, C. A., Giancolab, C., Baroneb, G. (2000). Crystal structure and conformational stability of N-acetyl-l-prolyl-l-leucinamide. Comparison between structural and thermophysical data. Journal of Molecular Structure, 553, 117–130.
- Rollet, J. S. (1965). Computing Methods in Crystallography. Oxford: Pergamon Press.
- Roothaan, C. C. J. (1951). New Developments in Molecular Orbital Theory. Review of Modern Physics. 23, 69-89.
- Sayre, D. (1952). The squaring method: a new method for phase determination. Acta Cryst., 5, 60-65.
- Sheldrick, G. M. (1998). SHELXL-97, A program for crystal structure refinement, University of Göttingen, Germany.

- Sheldrick, G. M. (1998). SHELXS-97, A program for crystal structure solution, University of Göttingen, Germany.
- Sparks, R. A. (1961). Computational Methods and Phase Problem in X-Ray Crystallography. Oxford: Pergamon Press.
- Spek, A. L. (1990). PLATON: Multi-purpose Crystallographic Tool. Acta Crystallographica, A46, C34.
- Stewart, J. J. P. (1989). J. Computational Chemistry, 10, 221.
- Woolfson, M. M. (1954). The statistical theory of sign relationships. Acta Cryst., 7, 61-64.
- Zachariasen, W. H. (1952). A new analytical method for solving complex crystal structures. Acta Cryst., 5, 68-73.
- Zhaoa, H., Weib, Y., Huaa, W. (2000). Synthesis, crystal structure and self-organization of molecules containing 2,5-bis(o-amino-phenyl)-1,3,4-oxadiazoles unit and N-tos-l-amino acid residues. Journal of Molecular Structure, 553, 109–115.